EXPERIMENTAL STUDY OF XUROGRAPHIC SPIRAL MICROCHANNEL HEAT SINKS

by

Ali Yasser Thamer

A thesis submitted to the faculty of
The University of Utah
in partial fulfillment of the requirements for the degree of

Master of Science

Department of Mechanical Engineering

The University of Utah

May 2014

The University of Utah Graduate School

STATEMENT OF THESIS APPROVAL

The thesis of **Ali Yasser Thamer**

has been approved by the following supervisory committee members:

Timothy A. Ameel	, Chair	**01/03/2014** Date Approved
Bruce K. Gale	, Member	**01/03/2014** Date Approved
Meredith M. Metzger	, Member	**01/10/2014** Date Approved

and by **Timothy A. Ameel** , Chair of the Department of **Mechanical Engineering**

and by David B. Kieda, Dean of The Graduate School.

ABSTRACT

An experimental study was performed to explore the possibility of constructing a spiral microchannel heat sink using a laser-based xurographic technology with double-sided adhesive Kapton® tape, which has a low thermal conductivity. Xurography is a rapid prototyping micromanufacturing technology that, in contrast to expensive and time-consuming traditional microfabrication technologies, enables the fabrication of inexpensive microfluidics devices in a short time frame. A set of three xurographic spiral microchannel heat sinks with different channel length, width, hydraulic diameter, aspect ratio, and number of spirals were fabricated, tested and analyzed. For all test sections, channel depth was determined by the Kapton® tape film thickness, which is approximately 105 μm. The heat sinks were experimentally tested at different flow rates and heat fluxes. Four sets of tests were performed on each heat sink. Distilled water, used as the working fluid, entered the test sections at room temperature (~22°C). The supplied heat ranged from 25 to 200 W, and the Reynolds number ranged from 200 to 1800. Results showed that the device with the widest channel (3 mm) extracts more heat than those with smaller widths and requires the least amount of driving pressure. The maximum heat dissipation rate for the devices was approximately 140 W, corresponding to a heat flux of approximately 10 W/cm². The maximum convection coefficient was on the order of 6500 W/m²/K and was achieved in the widest channel device with a corresponding Nusselt number of up to 2.2. Results indicate a thermal performance that is

less than desirable. Performance was adversely affected by the low thermal conductivity Kapton® tape and no enhancement due to secondary flows in the spiral geometry was observed. Comparison with a well-known macroscale curved duct correlation revealed a significant difference between the experimental results and predications.

To my parents and my family

TABLE OF CONTENTS

LIST OF FIGURES

LIST OF TABLES

NOMENCLATURE

α	Fluid thermal diffusivity (m^2/s)
A_c	Channel cross sectional area (m^2)
A_{th}	Channel heat transfer area (m^2)
C_p	Fluid specific heat ($kJ/kg/K$)
D_e	Dean number
D_h	Channel hydraulic diameter
D_r	Inlet and outlet reservoir diameter
ΔP	Channel pressure drop (kPa)
δR	Output uncertainty
ΔT	Temperature difference ($°C$)
f_c	Coiled channel friction factor
f_s	Straight channel friction factor
γ	Channel aspect ratio (H/W_c)
H	Channel height (mm)
h	Convection coefficient ($W/m^2/K$)
K	Fluid thermal conductivity ($W/m/K$)
L	Channel length (mm)
m	Fluid mass (kg)
$\dot{m}$	Fluid mass flow rate (kg/s)

μ	Fluid dynamic viscosity ($Pa.s$)
Nu	Nusselt number
υ	Fluid kinematic vescosity (m^2/s)
P	Heater measured power (W)
P_{max}	Maximum heaters power (W)
P_r	Prandtl number
Q	Heat rate (W)
q	Heat flux (W/m^2)
R	Channel curvature radius (m)
R_e	Reynolds number
ρ	Fluid density (kg/m^3)
t	time (s)
T_{ave}	Average fluid temperature ($°C$)
T_i	Inlet fluid temperature ($°C$)
T_o	Outlet fluid temperature ($°C$)
T_w	Wall temperature ($°C$)
U	Mean fluid velocity (m/s)
V	Measured voltage ($volt$)
W_c	Channel width (mm)
W_p	Distance between two channels (mm)
x_n	Independent variable

ACKNOWLEDGMENTS

I would like to offer my thanks and appreciation for all of those involved with my thesis study: First and foremost to Dr. Timothy Ameel for his invaluable instruction and assistance which proved to be an essential element in completing the in depth work and research required for my thesis. Thanks to Dr. Meredith Metzger and Dr. Bruce Gale for their involvement as members on my supervisory committee. Thanks to Dr. Bruce Gale for allowing me to use his lab equipment as well as Rahul Kolekar, Dan Torgerson, Lam Nguyen, and Sultan Alshareef for their previous studies on the fluid flow and heat transfer in xurographic microchannels. The information gained from their work definitely saved countless hours throughout this research. Special thanks to my colleague, Lam Nguyen, for his help and support. Last but not least, I would also like to thank Jeff Kessler, a staff member from the mechanical engineering department, for his technical support. I am extremely grateful for the continuous support and encouragement from my parents, family and friends.

CHAPTER 1

INTRODUCTION

1.1 Motivation

Heat transfer mechanisms depend on many factors. One of them is the physical size of the domain where the heat transfer takes place. That domain has been of interest to scientist for over 400 years. Size effects have more importance when dealing with systems of small dimensions [1]. As is well known, the most effective heat and mass transfer processes in the human body take place in the kidneys and lungs where the vessels approach a small size of approximately 4μm [2].

In the last few decades, modern microengineering applications have led to increased interest in microconduit physics; in particular, fluid flow and heat transfer [2]. Miniaturized mechanical systems have today found a foothold in many scientific and commercial fields such as medicine, drug delivery, bioengineering, chemical reactors, microelectromechanical systems (MEMS), microheat exchangers, and electronics cooling.

Many of the MEMS and microfluidic devices utilize microchannels to enhance convective heat transfer by taking advantage of the high surface area to volume ratio [2]. The rate of a transfer phenomenon, such as convection heat transfer, depends on the surface area, which varies with the channel diameter. Alternatively, the volume flow rate

varies with the flow cross sectional area. Consequently, the surface area to volume ratio varies inversely with diameter [2], suggesting that convective heat and mass transfer rates increase with a decrease in channel size.

Modern high performance integrated electronics generate high heat rates in a small area. Dissipating such high heat rates has increased the demand for novel heat dissipation methods. Current heat dissipation requirements in the electronics industry are on the order of 100 W/cm^2.

Microchannel heat sinks are a technology that can dissipate high heat rates; they take advantage of the microchannel feature of high surface area to volume ratio. Enhancing microchannel heat sink performance requires a good understanding of the physics of the forced convection heat transfer phenomenon.

There are many techniques that can be used to increase heat flux through forced convective heat transfer. Enhancement can be obtained by increasing the convection coefficient and/or convection surface area. Creating secondary flow in the channel can also increase heat transfer rates. For instance, a helically coiled tube will increase the convection coefficient by introducing centrifugal forces within the flow field. Those forces will induce secondary flows with tangential velocity components that increase flow speed near the tube wall [3]. Thus, one heat transfer enhancement technique involves the use of spiral channels. As noted, the spiral flow geometry induces secondary flows, which in turn increase the local convection coefficient.

The study reported herein sheds light on single-phase forced convection heat transfer in a spiral microchannel heat sink fabricated by laser-based xurography. Xurography, as introduced in the next section, is a rapid prototyping technology that

enables the fabrication of inexpensive microfluidic devices in a short time frame as compared to the expensive and time consuming traditional microfabrication technologies. Microchannel heat sinks can be used for aerospace applications, thermal control of film deposition, and for cooling of laser mirrors and avionics [4].

1.2 Introduction to xurography

In the first era of micromachining technology (over three decades ago), the fabrication methods that were used to produce microelectromechanical systems (MEMS), and later microfluidic systems, relied solely on conventional semiconductor materials and techniques primarily developed for integrated circuit manufacturing [5]. Initially, silicon was the dominant material used to produce MEMS along with other materials such as acrylic, glass and polydimethylsiloxane (PDMS) [6]. Devices manufactured from silicon have high geometrical precision; however, the fabrication technology requires sophisticated microfabrication equipment and facilities, which results in high cost and long production times. Techniques such as soft lithography are also expensive, since they too require devoted instrumentation, chemicals and cleanrooms.

As the demand for microfluidic applications grows, interest has increased for methods that may enable microfluidic systems to be fabricated in a rapid and inexpensive way. Fast and inexpensive methods will open the microfluidics field to a larger group of interested scientists and developers from various fields, especially if these disciplines do not require high precision devices.

A novel fabrication technology called xurography has been developed recently as an inexpensive rapid manufacturing method. Xurography originates from the Greek words that mean “razor writing.” Bartholomeusz et al. [7] first presented this method in

2005 as an alternative to the conventional expensive and time consuming technologies when precision was not a big concern for first stage prototyping. Xurography was first used in the graphic art industry to cut designs and shapes in adhesive vinyl films using a cutting plotter with a knife blade. Typical cutting plotters have an accuracy of approximately 10 μm with different settings and blade angles.

Microchannels can be made by xurography by first cutting the desired design in double-sided adhesive film. The cut parts of the film are then removed and the remaining tape is sandwiched between two substrates, which are usually glass. The channel height is equivalent to the film thickness, and the channel width is equivalent to the cut width. With a fixed channel height, the aspect ratio depends primarily on the channel width. Channels fabricated by xurography are hybrids; two walls are made out of substrate materials and the other walls are a combination of two layers of adhesive and the polyimide film (typically Kapton®).

Several researchers and scientists have reported that xurographic microstructure costs are negligibly small compared to the standard methods and that the process has a short fabrication time. One study shows a comparison between glass etching and xurographic prototyping of microchannels for DNA melting analysis. The study concluded that xurography is an effective and reliable prototyping method that can be used as an alternative to conventional glass etching technology [8].

Since xurography was first introduced for microsystem fabrication, several upgrades have been applied to overcome difficulties related to the creation of more complex geometric shapes such as curves and circles. One advance has been the replacement of the cutting plotter with a laser-cutting tool. A recent study shows how

laser based xurography can be utilized to produce a mask as part of the glass etching microchannel technology [9].

1.3 Summary

In the work reported herein, the laser based xurography microfabrication method will be used to produce a spiral microchannel heat sink from double-sided adhesive polyimide Kapton® tape sandwiched between two substrates. Kapton®, a polyimide film developed by Dupont, can remain stable over a wide range of temperatures. Kapton® is often used for flexible printed circuits and thermal micrometeoroid garments, i.e., the outside layer of space suits [10].

Since this study focuses on the thermal behavior of a spiral heat sink, the two substrates should have high thermal conductivity. For this reason copper was chosen.

Xurographic microchannels are suitable for low flow rates tests; however, the channels are typically limited to relatively low internal pressure since bonding is facilitated by only double-sided adhesive tape. It has been reported that devices with glass substrates are able to withstand internal pressures up to 172 - 207 kPa before failure due to liquid leakage between the two glass substrates and the adhesive layers [11]. To extend the pressure range for xurographic microchannel systems, additional force can be applied to the bonds through an external clamping system, as has been reported by Torgerson [11], Nguyen [12] and Kolekar [13].

As will be reported in Chapter 2, the two copper substrates in this study can also be used as part of an external mechanical clamping system by installing threading holes for clamping bolts.

This study was undertaken to answer several fundamental questions. These questions are related to the design, fabrication, and assembly of a microchannel spiral heat sink and to the performance of such a system for a wide range of operation conditions. Specific research questions include:

1. Can an effective spiral heat sink be constructed by xurography with Kapton® tape, which has low thermal conductivity?
2. What are the upper limits on temperature and pressure for such a system? The adhesive used for bonding is expected to become less effective at elevated temperatures and pressures.
3. Can a laser cutting system produce a spiral pattern with desirable resolution?
4. What is the minimum channel width that can be created with the laser cutting system?
5. What are the heat rates that can be dissipated as a function of the mass flow rate?
6. How does the channel design (length, width, number of spirals) affect thermal performance?

This document was written with the intent of generating a chapter that represents a manuscript that can be submitted for publication. Chapter 2 has been constructed with that objective in mind. The contents of that chapter include information on related work, the design process, the final design, fabrication, assembly, experimental procedure, data acquisition, data reduction, and results. Chapter 3 includes conclusions, and recommendations for future work.

1.4 References

[1] C. B. Sobhan, G. P. Peterson, Microscale and Nanoscale Heat Transfer Fundamentals and Engineering Applications, First ed., CRC Press, Boca Raton, Florida, 2008.

[2] S. G. Kandlikar, S. Garimella, D. li, S. Colin, M. R. King, Heat Transfer and Fluid Flow in Minichannels and Microchannels, First ed., Elsevier, Amsterdam, 2006.

[3] F. P. Incropera, D. P. Dewitt, T. L. Bergman, A. S. Lavine, Fundamentals of Heat and Mass Transfer, Seventh ed., Wiley, New York, 2011.

[4] P. Jiang, M. Fan, G. Si, Z. Ren, Thermal-hydraulic performance of small micro-channel and porous-media heat exchangers, International Journal of Heat and Mass Transfer 44 (2001) 1039-1051.

[5] Byung-Ho Jo, Linda M. Van Lerberghe, Kathleen M. Motsegood, David J. Beebe, Three-dimensional micro-channel fabrication in polydimethylsiloxane (PDMS) elastomer, Journal of Microelectromechanical Systems (2000) 76-83.

[6] C. Liu, Foundations of MEMS, First ed., Pearson Prentice Hall, Upper Saddle River, NJ 2006.

[7] D. A. Bartholomeusz, R. Boutte, J. Andrade, Xurography: rapid prototyping of microstructures using a cutting plotter, Journal of Microelectromechanical Systems 14 (2005) 1364-1374.

[8] J. Greer, S. Sundberg, C. Wittwer, B. Gale, Comparison of glass etching to xurography prototyping of microfluidics channels for DNA melting analysis, Journal of Micromechanics and Microengineering 17 (2007) 2407-2413.

[9] P. Santana, T. Segato, E. Carrilho, R. Lima, N. dossi, M. Kamogawa, A. Gobbi, M. Piazzeta, E. Piccin, Fabrication of glass microchannels by xurography for electrophoresis applications, The Royal Society of Chemistry 138 (2013) 1660-1664.

[10] Kapton is a polyimide film developed by DuPont that remains stable across a wide range of temperatures. Found at: http:// en.wikipedia.org/wiki/Kapton.

[11] D. Torgerson, Microscale loss coefficients through expansion and contraction xurographic microchannels, MS thesis, University of Utah, Salt Lake City, UT, 2010.

[12] L. Nguyen, Contraction/expansion effects in 90° miter bends in rectangular xurographic micro-channels, MS thesis, University of Utah, Salt Lake City, UT, 2011.

[13] R. Kolekar, Fluid flow characteristics in xurographic microchannels, MS thesis, University of Utah, Salt Lake City, UT, 2009.

CHAPTER 2

XUROGRAPHIC SPIRAL MICROCHANNEL HEAT SINKS

2.1 Introduction

As the demand for microfluidic systems grows, the need for technologies that enable rapid prototyping of first designs is also increasing. In the development phases of a project the ability to generate an idea, create a design, and fabricate a prototype quickly (in a day or so) is highly desired. At the same time, this technology should be relatively inexpensive in both first cost and in use so a designer is free to create as many prototypes as desired. In 2005, a novel fabrication technology called xurography was first introduced by Bartholomeusz et al. [1] as a technology for microchannel fabrication. This system has proven to be economical, efficient, and an effective alternative to the conventional expensive and time-consuming fabrication technologies.

While the cost of xurographic microstructures is negligibly small compared to the standard methods, and xurography has a short fabrication time, the heat transfer characteristics of such devices must be investigated to properly design and manufacture a xurographic microchannel heat sink.

Microchannel thermal and hydrodynamic performance was first investigated in the pioneering work of Tuckermann and Pease [2] in 1981. They discovered that reducing the size of the flow domain to the submillimeter regime drastically boosts the heat

transfer rate. They proved that the microchannel heat sink is a highly efficient cooling device capable of dispersing heat at rates up to 790 W/cm² with a maximum substrate temperature rise of 71°C above the coolant entering temperature. Since Tuckermann and Pease's early work, research in the microchannel heat sink field has been growing rapidly.

Following their research, a number of studies were conducted to explore microchannel physics with one central question: is it possible to apply the macroscale fluid flow and heat transfer continuum governing equations and correlations in the microscale domain?

Wu and Little [3], in 1984, conducted a heat transfer experiment for gas flow in a trapezoidal fine channel heat exchanger with a hydraulic diameter in the range of 55-76 μm. They observed that fluid flow and heat transfer both behave differently than in conventionally sized channels. They proposed an empirical correlation to calculate the Nusselt number *Nu* in the turbulent regime where the Reynolds number *Re* is greater than 3000.

Pfahler et al. [4] experimented on the fluid flow characteristics of extremely small rectangular microchannels, which have a cross sectional area ranging from 80-7200 μm^2. They indicated that the microchannel flow showed considerable deviation from characteristics predicted by the Navier-Stokes equations. Peng et al. [5, 6, and 7] performed experimental investigations on the heat transfer performance of straight microchannels fabricated from stainless steel plates. Channel width ranged from 0.1-0.6 mm, and the depth was in the range 0.2 - 0.7 mm. Their results indicated that microscale fluid flow and heat transfer differed from conventional correlations and that a transition

to turbulent flow occurred at a much lower Reynolds number than for conventionally sized channels. They pointed out that the channel arrangement has critical influence on heat transfer rate.

Sobhan and Garimella [8] completed a comparative study of almost all of the published literature up to 2001 for single-phase fluid flow and heat transfer performance of microchannels, microtubes and minichannels. They created a summary table containing detailed information on the studies reviewed, such as: configuration, parameters, nature of work, observations and conclusions along with predictive correlations. They observed contradictions with conventional macrochannel theories. They concluded that investigators rarely agreed in their predictions. They proposed several sources that could cause the differences, such as nonuniformity of channel dimensions, nature of thermal and flow boundary conditions, entrance and exit effects, surface roughness, uncertainties and errors in instrumentation measurement, and measurement locations.

Morini [9] provides a detailed review of the experimental results of single-phase flow and heat transfer in microchannels. In this review, he critically analyzes the friction factor and Nusselt number in channels that have a hydraulic diameter of less than 1 mm. He stated that in many of the studies the experimental results that describe the analyzed variables diverge from the standard equations. At the same time, those results appear to conflict with each other. He suggested several reasons to explain these discrepancies such as viscous dissipation, property variation, electro-osmotic effects (EDL), rarefaction, compressibility, relative roughness and experimental uncertainties.

In the last decade, researchers have reached a stage where convergence between micro- and macrochannels physics is apparent.

Lee et al. [10] performed an experimental investigation testing the validity of the use of conventional correlation to examine the thermal performance of deionized water flow through rectangular microchannels made of a machined copper. The hydraulic diameter ranged from 318 to 903 μm, and the Reynolds number ranged from 300 to 3500. They numerically modeled these channels based on the classical continuum approach, utilizing the 3D conjugated method and simplified thin wall procedure. Their numerical results agreed with the empirical data for precisely simulated inlet and boundary conditions.

Owhaib and Palm [11] experimentally investigated the heat transfer performance of refrigerant R134a in microtubes with diameters of 0.8, 1.2 and 1.7 mm. Experimental data were compared to well-known macroscale equations and other correlations that could apply to microchannels. Their result showed good agreement with conventional predictions. At the same time, there was no consistency between the experimental data and the proposed equations for microchannels. Heat transfer coefficients were nearly identical in the laminar flow region for all tested tubes.

Qu and Mudawar [12] numerically studied fluid flow and heat transfer characteristics of water in rectangular silicon microchannel heat sinks by employing the finite element method and the SIMPLE algorithm. Microchannels dimensions were 57μm wide and 180μm deep. They compared their numerical results to the published data. They reported that the temperature change in the solid and fluid along the length varied linearly

and that *Nu* is much larger near the channel inlet. It was also reported that the flow did not become fully developed within the heat sink for a relatively high *Re* of 1400.

Gamrat et al. [13] numerically investigated the influence of conduction and entrance effects on laminar water flow and heat transfer in very high aspect ratio rectangular microchannels with spacing distance ranging between 0.1 and 1 mm, and a Reynolds number ranging from 200 to3000. In contrast to their previous experimental work, the numerical results did not detect any noticeable scale effect on microchannel thermal performance.

Thermal management of higher density integrated circuits and high performance electronics requires the use of an innovative microchannel heat sink to dissipate the high heat rate. This innovation is possible by employing two different techniques to increase heat transfer rate, according to Naphon and Wangwises [14]. These mechanisms are both active and passive; active techniques regard the use of an external force to implement such augmentation, while passive methods utilize fluid additives or special channel configurations, which are simpler, cost less and do not conflict with other parts in the system [14]. In some of the heat sink literature, experiments with special channel geometries have been described [15].

Wang and Ding [16] experimentally investigated the heat transfer characteristics of a novel microchannel heat sink containing parallel longitudinal microchannels etched in a silicon base and transverse microchannels electroplated on a copper heat spreader. Each tiny transverse channel is 400μm long, 100μm wide and 20μm deep. They reported that the heat sink has high local heat transfer efficiency with enhanced overall heat transfer rate and that the temperature distribution was uniform over the heat sink area.

Heymann et al. [17] performed a numerical study to optimize pressure drop and flow power in fractal-like branching microchannel heat sinks. Numerical simulation was employed to study the shape effect on microchannel heat sink thermal and hydrodynamic performance by Mohammed and Shuaib [18]. They examined three different shapes: zigzag, curvy and step with the same cross-sectional area. They noticed that the biggest improvement for the heat transfer coefficient was achieved with the zigzag shape channel. At the same time, this shape had the highest pressure drop, friction factor, and wall shear stress.

Liu et al. [19] carried out an experiment to test the effect of longitudinal vortex generators on heat transfer and pressure drop in rectangular microchannels. The Reynolds number ranged from 170 to 1200, with the hydraulic diameter equal to 187.5μm and an aspect ratio of 0.067. They reported that thermal performance was improved by 9-21% when the flow was laminar and by 39-90% when the flow was turbulent. Pressure drop increased considerably, up 34-169% for the same flow range. This boost in heat transfer rate is due to the use of a different number of vortex generator pairs with different angles of attack. Based on their results they proposed an empirical correlation to calculate *Nu* and friction factor in the laminar and turbulent regimes. One of several passive enhancement methods is the use of curved conduits, which have been used in many thermal applications [14]. There are three different types of curved conduits: helically coiled, spirally coiled and other coiled conduits [14]. Flow through curved channels is more complex due to the addition of centrifugal force. This supplementary force leads to the formation of secondary flows within the flow field, which in turn have significant impact on heat and mass transfer enhancement. The first investigation that studied flow

characteristics in curved pipes was performed by Dean [20, 21]. White [22] numerically investigated flow pressure drop through a constant curvature coil. Thangam and Hur [23] numerically studied the emergence and evolution of secondary flow in curved rectangular ducts by using the finite-volume method. They developed a correlation to calculate friction factor as a function of the Dean number *De* and duct aspect ratio. Good agreement was obtained between suggested equations and available experimental and computational results.

Downing and Kojasoy [24] performed an experimental investigation to develop correlations that characterize heat transfer and pressure drop in a miniature spiral cold plate heat exchanger due to the single and two-phase flow of refrigerant R134a. Comparison with well-known correlations showed a reasonable fit for low Reynolds number flow and an over prediction at higher Reynolds numbers.

Naphon and Wongwises [25] conducted an experimental and numerical study on the thermal behavior of a spiral coil heat exchanger under cooling and dehumidifying conditions. Reasonable agreement was observed between the experimental and theoretical predictions.

Yang et al. [26] reported experimental and theoretical predictions of the friction factor in curved microchannels. Considerable variation between experimental results and theoretical predictions was reported. Naphon and Wongwises [14] presented a detailed literature review of the published materials up to 2004 for flow and thermal behavior in curved tubes along with reported correlations. However, they noticed that references to studies on spirally coiled tubes are limited. Chu et al. [27, 28] found that their experimental friction factor and pressure drop data were in good agreement with

simulations based on the Navier-Stokes equations for laminar liquid flows through curved rectangular microchannels. After carefully studying the available literature, it is clear that studies on the subject of fluid flow and heat transfer characteristics in spiral microchannels are scarce.

In more recent years, a few studies related to spiral microchannels were conducted to identify the thermal and hydrodynamic performance.

Fan and Hassan [15] numerically studied the cooling performance of a swirl microchannel heat sink with different curvatures and channel numbers. They showed that increasing curvature and the number of channels can improve the cooling effect at a fixed inlet flow rate. A recent study on flow and heat transfer in swirl microchannel heat sinks performed by Xi et al. [29] showed that the spiral geometry is capable of enhancing the heat transfer rate up to 50% compared to a straight microchannel. In their experiment they used a 30% ethylene glycol solution as a coolant. The channel hydraulic diameter ranged from 0.3-0.8 mm. A comparison between their results and conventional correlations indicates a clear deviation. Ghobadi and Muzychka [30] performed an experimental and analytical study on the heat transfer in a spiral microchannel heat sink with a 1 mm hydraulic diameter. Liquid coolants were water and four silicon oils. No important performance changes were reported by switching the flow inlet port from the middle to the side of the heat sink.

The study reported herein, was undertaken to answer the questions given in Chapter 1. In addition, xurography has been used very rarely to construct microchannel heat exchangers and heat sinks. To the author's knowledge, xurography has not been used previously to fabricate a spiral microchannel heat sink. The current study is

designed to explore the thermal performance of a xurographic microchannel heat sink with a passive enhancement feature, namely the spiral geometry. The performance of the heat sink is evaluated in terms of overall heat flux, heat rate, convection coefficient and Nusselt number. The pressure drop through the channels is also measured to assess the energy input required to enable the convective processes. These performance parameters are evaluated for different channel geometries, which include various channel widths, aspect ratios, and length. In addition, the coolant (water) flow rate is also varied to produce a range of Reynolds numbers and Dean numbers.

2.2 Heat sink predesign analysis

The first step in the design process is to understand the impact of various geometrical factors and operating conditions on device performance in conjunction with the effects of the material properties and manufacturing limitations.

Two models, one analytical and the other numerical, were created to investigate these effects. In these two models, conventional correlations for macroscale coiled ducts were employed to simulate the fluid flow and heat transfer processes. Several simplifying assumptions were applied in both models, specifically:

1- Steady fluid flow and heat transfer.

2- Laminar flow.

3- Incompressible fluid.

4- No-slip boundary conditions.

5- No heat losses to the surrounding space.

2.2.1 Analytical model

A preliminary analytical model was created using Matlab software to simulate the pressure drop and heat transfer in spiral xurographic microchannels with different lengths and widths. Table 2.1 summarizes the geometrical parameters for the channels used in this analysis. Channel depth was set to be constant in all cases at 0.105 mm, as will be discussed later in the design and fabrication section. Water properties, such as density, viscosity, and thermal conductivity were calculated from Robert C. Weast [31] as a function of the average water temperature.

Two well-known correlations were employed to predict the thermal and hydrodynamic behavior of the microchannels. Dravid et al. [32] proposed a correlation to predict the thermal behavior of a laminar flow in helically coiled tubes operating in the thermal entrance region. In this correlation Nusselt number *Nu* is defined as a function of the Dean number and Prandtl number.

$$Nu = (0.65\sqrt{De} + 0.76)\, Pr^{0.175} \text{ for } 50 \leq De \leq 2000 \text{ and } 5 \leq Pr \leq 175 \qquad (2.1)$$

Dean number is a dimensionless parameter, which is defined as

$$De = Re\left(\frac{D_h}{2R}\right)^{1/2} \qquad (2.2)$$

where *Re* is the Reynolds number, D_h is the hydraulic diameter, and *R* is the channel curvature radius. These parameters are defined in detail in section 2.5.

It is clear that the channel curvature radius changes continuously along the channel length, which in turn causes the value of the Dean number to vary also. To deal with this issue, a discretization method [30] is utilized, as described in section 2.5.

The Prandtl number is defined as

$$Pr = \frac{\upsilon}{\alpha} \qquad (2.3)$$

where υ is the kinematic viscosity, and α is the thermal diffusivity.

There was no intent to test actual devices in the turbulent flow range due to the high pressure drop associated with the water flow in this region; therefore, the thermal pre-design analysis for turbulent flow was not conducted. It was reported by previous xurographic microchannel studies [33, 34, 35] that the water flow in a straight xurographic channel is associated with high pressure drop, and this type of microchannel can withstand a pressure drop up to 2500 kPa [33]. As described in the following paragraph, the xurographic spiral microchannel requires high pressure to drive the coolant through the channel in the laminar flow region.

Figure 2.1 shows the expected thermal performance in terms of *Nu* for the spiral microchannels at different Reynolds numbers.

White [22] proposed a correlation to estimate the friction factor for laminar flow in coiled ducts as a function of the Dean number, and channel aspect ratio.

$$\frac{fc}{f_s} = \left(1 - \left[1 - \left(\frac{11.6}{De}\right)^{0.45}\right]^{\frac{1}{0.45}}\right)^{-1} \quad \text{for} \quad 11.6 \leq De \leq 2000 \tag{2.4}$$

where f_c is the friction factor for the coiled channel, f_s is the friction factor for a straight channel, and *De* is defined in equation 2.2 in terms of *Re*. The friction factor for laminar flow in straight channel fs is determined according to Shah and London correlation [41] as:

$$f_s = 96\,[1 - 1.3553\gamma + 1.9467\gamma^2 - 1.7012\gamma^3 + 0.9564\gamma^4 - 0.2537\gamma^5] / Re \tag{2.5}$$

where γ is the channel aspect ratio.

The pressure drop in all channels was calculated as.

$$\Delta P = f_c \frac{L}{D_h}\frac{\rho U^2}{2} \times 10^{-3}\ \text{(kPa)} \tag{2.6}$$

Figure 2.2 shows the predicted pressure drop for different channel lengths and widths in the laminar flow region. It is evident from Figure 2.1 that the three different channels thermally behave in nearly the same manner, and they show almost the same thermal performance in terms of the Nusselt number at the same Reynolds number value. Therefore, the pressure drop predictions from Figure 2.2 drive the decision about the channel size that will be adopted in this experiment. Figure 2.2 shows that the first channel has the highest pressure drop at the same Reynolds number, and it has nearly double the pressure drop of the third channel. The first channel also is the narrowest, longest, and the one with the largest number of spirals, as can be seen in Table 2.1. As a result, the smallest channel width that is used in an actual device is 1 mm. Even with the high pressure drop associated with the long channel, which has 4.5 spirals, it was not possible to reduce the length and number of spirals, because it was preferable to have a wide channel with reasonable surface area (thermal area) that covers the substrate footprint in order to extract more heat.

2.2.2 Numerical model

A three-dimensional conjugate heat transfer model was used to simulate laminar convective heat transfer of water flows in a xurographic spiral microchannel heat sink, as illustrated in Figure 2.3. The heat sink is assumed to be constructed from two square copper blocks and a spiral microchannel cut from a square piece of a Kapton® polyimide film. All three components had a 50 mm X 50 mm cross sectional area. The two copper plates are 3 mm thick each, and the Kapton® polyimide layer is 0.1 mm thick. Channel dimensions are: 1 mm width, 0.1 mm depth, and 260 mm length. The simplifying assumptions that were stated earlier were used in this model. In this experiment, it is

understandable that it is difficult to acquire a direct measurement for the channel wall temperature; thus, it is important to find an appropriate location or locations from which a good approximation of that temperature can be made. In order to do that it is necessary to know the heat flux and temperature distribution in the vicinity of the microchannel. This was the main reason behind creating this model. The method of measuring the microchannel wall temperature indirectly has been used by several researchers [5, 10, 19, 29, 30, and 42] in studies similar to the current study.

COMSOL Multiphysics commercial software was utilized to create this model. COMSOL employs the finite element method to solve the governing equations for a given physical domain and boundary conditions. Due to the complexity of the fluid flow and heat transfer physics in the spiral microchannel heat sink, it was not possible to simplify the simulation procedure by using a two-dimensional model. For this reason, it was necessary to create a three-dimensional model.

Using the COMSOL tools and libraries, three different domains were built for water, polyimide tape, and the copper blocks. Materials with temperature independent properties were assigned to those domains.

An adiabatic boundary condition was applied to all the exterior surfaces, except the bottom surface where a uniform heat flux was applied. A uniform velocity with a constant water temperature was assigned at the channel inlet. No-slip boundary conditions were used at all the channel walls. The outlet of the channel was set to a "pressure, no viscous stress'' boundary condition with zero outlet pressure. A mesh dependency study revealed that the mesh size in the water domain has greater impact on the overall result than in the other domains. During this process, the mesh was refined to

the extent where results became mesh independent. After each model had been solved, it was validated by a first law of thermodynamics analysis in which the amount of heat extracted by water was compared to the heat flux applied to the bottom surface. In every case, the expected energy balance was confirmed. The default COMSOL convergence criteria were used in the solution process.

To conduct the experimental heat sink performance analysis, essential variables should be measured precisely; one of these variables is the channel wall temperature. As will be explained more thoroughly in the experimental setup and test procedure section, eight thermocouples are inserted in the copper substrates at carefully selected spots to obtain an average channel wall temperature measurement; copper represents 90-96 % of the channel wall area. To achieve an accurate measurement and to determine where the thermocouples should be placed, the temperature distribution through the device should be known a priori. Figure 2.4 shows the heat flow through the device, while Figures 2.5 and 2.6 illustrate the temperature field of two surfaces 2 mm above and below the channel stratum. In Figures 2.4, 2.5 and 2.6 the cold refrigerant is entering at the center of the spiral at a temperature of 5°C. The lower copper substrate is heated from below with a constant heat flux of 1.2 W/cm^2 and all other perimeter surfaces are adiabatic. As expected, heat flows upward toward the cooler fluid in the microchannel. The heat flow meets with thermal resistance at the Kapton tape layer, as evidenced by the sharp slope changes in the isoflux lines. Heat flows to the cold fluid inlet region as expected. The isothermal data indicate that a 3.6°C and 4.3°C maximum temperature difference occurs in the solid above and below the channel layer, respectively. These data suggest that properly placed thermocouples (locations described in the next section) could provide a

reasonable average wall temperature for the data analysis. Note that the solid temperatures are well below the anticipated maximum operating temperature of the adhesive (75°C) based on prior experiments [33, 34]. For these conditions, the coolant outlet temperature is 18°C, indicating a channel with this design is capable of dissipating 5.25 W/cm^2 of heat with a fluid temperature rise of 13°C.

2.3 Heat sink design and fabrication

Each heat sink tested in this investigation consists of 1) a Kapton layer with a spiral microchannel 2) a base copper substrate, and 3) a copper cover plate. All three components had a 76 mm x 76 mm cross sectional area. Copper was chosen for the substrate and cover due to its high thermal conductivity. To provide sufficient rigidity when clamped, the cover plate is 16 mm thick. The lower substrate is 40 mm thick. This size allows for the insertion of cartridge heaters and sufficient depth for the threaded bolt holes associated with the clamping system. Each of the 12 bolt holes is 15 mm deep and is threaded for Socket bolts, each with a 6 mm diameter coarse thread, 20 threads per inch, and 1 mm thread pitch. The bolts are arranged around the perimeter of the cover and substrate, approximately 5 mm from each edge. The cover has a 1.6 mm through hole 3.5 mm from the dead center that serves as the inlet port (for reverse flow, it serves as the outflow port). A second 1.6 mm through hole that serves as the outlet port is located 26 mm from the inlet port in the radial direction. The microchannel spiral design was laser cut into 76 mm x 76 mm pieces of double-sided adhesive Kapton tape. Two circular reservoirs with a diameter greater than the microchannel width were cut into the tape at the start and end of the spiral. These circular regions served as inlet and outlet reservoirs, respectively.

AutoCAD software was employed to draw the three spiral microchannels. Drawings were saved in .dwg format and transferred to the laser plotter for the cutting process. In this work, the spiral microchannels were constructed using the xurographic method. The spiral pattern was cut in double-sided adhesive Kapton® tape, which is made out of a single Kapton® polyimide layer sandwiched by two silicone adhesive layers. The total thickness of the tape is approximately 105 μm.

The geometric parameters for the spiral microchannels are listed in Table 2.2. Details of the heat sink are shown in Figure 2.7.

The copper pieces were machined form copper bar stock. The copper substrate is 76 mm long x 76 mm wide x 40 mm thick. Two holes were drilled on one side of the block; each has a 9.6 mm diameter and is 63.5 mm long, with sufficient tolerance to easily install two cartridge heaters. The hole center were located 20 mm below the microchannel layer. The two heaters (Omega CIR 20207, 500W, 120V, 2 inches long, and 3/8 inch diameter) were used as the heat source during the tests. Twelve 6.35 mm holes were drilled along the perimeter of the substrate, approximately 5 mm from the edge; each has a 6 mm (1/4 in) thread. These holes were used in the final assembly to fasten twelve 6 mm (1/4 in) bolts, which form a clamping system that provides a uniform, well distributed force on the test section and minimizes potential risk of leakage.

Using the information from the numerical predesign analysis, four 1.6 mm diameter holes were drilled, one on each of the sides of the substrate. Each hole is 20 mm long and is centered between the vertical edges 3 mm from the upper surface. Four thermocouples were installed in these holes; their average reading represents the temperature of the channel lower wall.

The top copper plate is 76 mm x 76 mm x 16 mm. Two through holes were drilled through this piece; each has a 1.6 mm diameter; 7 mm threads were added to the 1.6 mm holes for the installation of Swagelok fittings. These two fittings were utilized as the inlet and outlet ports. Four other holes were drilled on the upper surface in the center of each quadrant. Each 1.6 mm diameter hole is 14 mm long. Four thermocouples were installed in these holes. Holes locations were determined as a direct result of the numerical pre-design analysis to give the best representation of the temperature of the channel upper wall. The bottoms of these holes are 2 mm from the lower surface of the cover plate. Twelve additional 6.35 mm (1/4 in) holes were drilled through the cover along the perimeter at locations aligned with the threaded holes in the substrate. After the machining processes, a milling machine was used to deburr the pieces. Subsequently, each piece was polished in an Allied M-Prep3 spinning disk polishing machine. Final smoothing was completed with a looping machine using boron carbide suspended in an oil-base gel. The two pieces were then washed with distilled water and isopropyl alcohol, dried, wrapped in a smooth piece of cloth and set aside for final assembly. Detailed information about the polishing process can be found in Fathiel [33], and Alshareef [34]. Figure 2.8 presents a photograph of the machined and polished copper pieces.

The tape was first bonded to the upper surface of the copper substrate and then loaded into a Universal laser-plotting machine, model VL3.60. The laser cutting machine has variable beam power, cutting speed, and beam density settings. An appropriate setting based on a previous study conducted by Fathiel [33] was used to cut the Kapton® tape. A detailed explanation about the laser plotter use for cutting Kapton® tape can be found in Fathiel [33]. The cut section was removed and soot produced by laser heating

was rinsed away with water. The remaining portion of the tape forms a channel between the two copper surfaces. The penultimate step was bonding the cover plate to the substrate. This step required aligning the 1.6 mm inlet and outlet holes in the cover plate with the reservoirs in the tape. Finally, the test section adhesive was cured in an oven at 65°C for 1 hour [35, 37]. Figure 2.9 shows the cut tape on the top of the substrate, and removal of cut tape.

Temperature readings were taken at the inlet and outlet ports to measure fluid entry and exit temperatures, respectively. Another eight temperature readings were taken in the copper substrate and cover to determine the channel wall average temperature. Specific locations for the temperature sensors are shown in Figures 2.7, 2.8 and 2.10. Pressure sensors were placed in the connecting tubing 50 cm upstream of the inlet port and 46 cm downstream from the outlet port. The pressure measurements were used to determine pressure drop in the system. It is understood that minor losses associated with the contraction, expansion, and 90° bends are included in the pressure drop; however, pressure drop was used primarily for an overall assessment of system performance. Thus, the pressure drop in just the microchannel is not required.

During the current study, three heat sinks with different channel patterns were tested. Since these patterns were created in the tape, only the tape was replaced for each test. The two copper pieces were cleaned, polished and re-used. Figure 2.10 shows the final assembled device.

2.4 Experimental setup and test procedures

An open flow loop was utilized in this investigation with distilled water as the working fluid. This type of flow loop was used by Lee et al. [10] and found to be

preferable to the use of a pump due to the steady and smooth flow it provided along with a wide range of Reynolds numbers. Figure 2.11 shows a schematic drawing of the experiment setup.

Water was pumped through the flow loop using a Parker piston-type accumulator (3.785 L, 101.6 mm bore) pressurized by a type K nitrogen tank. Pressure to the accumulator was controlled by a Tescom pressure regulator. A Gast Vacuum pump and a water supply tank were used to refill the accumulator with distilled water. A stainless steel piston divided the accumulator bore into two variable volumes; one filled with compressed gas, supplied from the nitrogen tank, the other filled with distilled water, provided by the water supply tank. The accumulator was connected to the vacuum pump and water tank with stainless steel tubing. Two Swagelok three-way valves were employed to control the delivery of water in and out of the accumulator, as shown in Figure 2.11.

A water filter (7 μm) was installed in the line leaving the accumulator. The filter is designed to prevent solid contaminants from entering the test section. This particular flow loop arrangement was utilized in studies recently conducted by Nguyen [35], Torgerson [36], and Kolekar [37].

Stainless steel tubing, PEEK tubing, Upchruch fittings, Swagelok fittings and P-728 adapters were used to connect the test section to the flow loop. Two four-way unions were placed upstream and downstream of the heat sink. The inlet and outlet flow pressure were measured at these unions using Setra 522 series pressure sensors, which have an uncertainty equal to ± 0.15% of full scale. The sensors were powered by a PMC DC power supply.

The inlet and outlet water temperatures were measured using type-T shielded thermocouples with an uncertainty of ± 0.5°C. Thermocouples were positioned approximately 10 cm from the inlet and outlet ports using P-728 three-way unions and U-288 male/male couplers to contribute to a more accurate temperature measurement, according to Alshareef [34]. Eight type-T thermocouples were inserted to the copper body to provide data used to determine the average microchannel wall temperature. Downstream from the test article, water was collected in a 600 g plastic beaker placed on a Scientific SL600 mass balance. The mass measurement and time, measured by a LabView internal clock, were used to determine the mass flow rate. The uncertainty in the balance and internal clock are ± 0.01 g and ± 0.01 s, respectively. A Swagelok needle valve was used to precisely control the flow rate.

Two Omega cartridge heaters were used as the heat source with maximum power input of 1000 W. An AC power supply (Variac) controlled the cartridge heaters and power was computed from a correlation provided by the heater manufacturer. This correlation will be discussed in details in section 2.5. Heat generated by the cartridge heaters is first transferred to the copper by conduction and later extracted by the distilled water, which is pumped through the spiral microchannel.

All the extracted data from the mass balance, thermocouples, pressure sensors, voltmeter, and internal clock were acquired, recorded and saved by a National Instruments PX-1010 data acquisition system with LabView software. Steady state was generally reached in 30 - 90 min for all tests performed in this investigation. Time to steady state depended on the mass flow rate and the level of power supplied to the heaters.

An Omegatherm® thermally conductive silicone paste was utilized to reduce the thermal resistance between the cartridge heaters and the copper substrate. For the same reason, the paste was applied to the thermocouples upon insertion into the cavities in each of the copper sections.

Before a test was conducted, a leakage check was performed for each heat sink. Because of the dynamic and thermal stresses exerted on the Kapton tape separation wall during operation, a water leak could occur as a result of adhesive failure. Therefore, each test section was pressurized with water up to 2413 kPa (350 Psi) with the clamping system loosened. Test sections that passed the leak test were then used for the heat dissipation studies. Figure 2.12 shows a photograph of the experimental setup.

2.5 Data reduction

The data sets extracted from the experiment are employed in a Matlab data reduction code to determine the desired parameters, such as the Reynolds number *Re*, heat rate *Q*, heat flux *q*, average heat transfer coefficient *h*, Nusselt number *Nu*, and Dean number *De* along with their associated uncertainties. The mass flow rate $\dot{m}$ is determined by

$$\dot{m} = \frac{m_2 - m_1}{t_2 - t_1} \tag{2.7}$$

where the mass *m* is measured by the mass balance, and the coincidence time *t* is recorded by the LabView internal clock. A condition is set to keep the relative uncertainty of the mass flow rate less than or equal to 0.1 % in order to filter the processed data in a manner that maintains the uncertainty value minimized in all the final outputs. In the data reduction code, the experimental data are selected first by determining the required time interval between mass measurements such that the mass

flow rate relative uncertainty value meets the condition stated above. The experimental uncertainty in the output parameters was calculated according to Moffat method [38]; this method will be explained in section 2.8. The measured temperature and pressure values are averaged for the time intervals where the relative uncertainty of the mass flow rate meets the specified condition. Water thermodynamic and transport properties such as density ρ, dynamic viscosity μ, specific heat at constant pressure c_p, and thermal conductivity k are determined from Robert C. Weast [31] as a function of the averaged water temperature T_{ave}, which in turn is defined as

$$T_{ave} = \frac{T_o + T_i}{2} \tag{2.8}$$

where T_o and T_i represent outlet and inlet coolant temperatures, respectively. These temperatures are measured at the inlet and outlet ports to assure a more accurate temperature measurement, as suggested by Alshareef [34].

The Reynolds number is traditionally defined as the ratio of the inertia force to the viscous force

$$Re = \frac{\rho U D_h}{\mu} \tag{2.9}$$

where the flow average velocity U is obtained from the mass flow rate relation as

$$U = \frac{\dot{m}}{\rho A_c} \tag{2.10}$$

and A_c is the microchannel cross sectional area. For a rectangular channel, the hydraulic diameter D_h is defined as

$$D_h = \frac{2(W_c \times H)}{W_c + H} \tag{2.11}$$

where W_c and H are the microchannel width and height, respectively. The power supplied to the cartridge heaters is calculated using an equation provided by the cartridge heater manufacturer

$$P = P_{max}\left(\frac{V^2}{120}\right) \tag{2.12}$$

where P_{max} is the maximum power the heaters can provide, and V is the supplied voltage measured with a LabView voltmeter, module number PXI/PCI-4060.

The heat generated by the cartridge heaters is first transferred to the copper blocks by conduction and later extracted by the distilled water, which is pumped through the spiral microchannel. The heat rate Q gained by the water is calculated from the first law of thermodynamics applied to the microchannel

$$Q = \dot{m}c_p\,(T_o - T_i) \tag{2.13}$$

The microchannel heat flux is calculated as

$$q = \frac{Q}{A_{th}} \tag{2.14}$$

The average convection heat transfer coefficient is defined as

$$h = \frac{Q}{A_{th}(T_w - T_{ave})} \tag{2.15}$$

where T_w is the average wall temperature taken as a mean of the eight embedded thermocouple readings. As explained in section 2.4, two groups of four thermocouples each were used to acquire the upper and lower wall temperatures. For each group of four thermocouples, the temperature variation is less than ±0.5 °C. This temperature difference is less than the instrument uncertainty, as shown in Table 2.3. The low disparity in thermocouple readings is attributed to the high thermal conductivity of copper. At the same time, the data sets demonstrate a notable temperature difference

between the substrate and cover plate. This distinction has an impact on the heat sink performance, as will be discussed in detail in section 2.8.

A_{th} represents the heat transfer surface area, defined as

$$A_{th} = 2L\,(H + W_c) \tag{2.16}$$

where L is the total microchannel length. In some of the previous experimental studies, researchers defined the heat transfer area in several different ways. In their calculation of the convection heat transfer area, Lee et al. [10] neglected the upper channel wall, as it was made out of acrylic, while the microchannel was machined into the top surface of a copper block. Xi et al. [29] used the same approach as Lee et al. [10] to define the heat transfer area. Recently, in two xurographic microchannel studies, performed by Fathiel [33] and Alshareef [34], heat transfer surface area was designated as the upper and lower channel surfaces only, and the Kapton® tape surface area was neglected because of its low thermal conductivity. In the current study, due to the presence of a temperature gradient normal to the Kapton® tape layer, a decision was made to include the small surface area of the tape along with the copper surfaces.

In the heat transfer process, the Nusselt number is the ratio of convective to conductive heat transfer rates. The average Nusselt number for the water pumped through the spiral channel is computed as

$$Nu = \frac{hD_h}{k} \tag{2.17}$$

To account for the influence of channel curvature on the heat sink performance, the Dean number should be calculated. The Dean number is a dimensionless parameter, defined in section 2.2 as

$$De = Re\left(\frac{D_h}{2R}\right)^{1/2} \tag{2.2}$$

where R is the spiral curvature radius. It is clear that this radius changes continuously along the channel length, which in turn causes the value of the Dean number to vary also. To deal with this issue, a discretization method [30] is utilized. In this method, the channel length is divided into small cells, the Dean number is calculated for each cell, and finally the sum of all Dean number values is divided by the total number of cells, resulting in the average Dean number. For this study, the typical cell size is 0.5 mm.

2.6 Characterization

For all three devices, a laser-based xurography technique was used to cut the spiral microchannel shape out of the double-side adhesive tape. This technique was used recently by Fathiel [33] to produce a cross-flow microchannel heat exchanger with multiple parallel channels. Fathiel discovered that using the laser beam to cut the double-side adhesive tape creates burnt or singed edges. The burnt edges make precise measurement of microchannel dimensions difficult. However, Fathiel did discover optimum laser settings for power, density and speed that produces the minimum amount of burnt material on the channel edges while also avoiding scratching the substrate; this study used Fathiel's laser settings. Due to the imprecision of channel measurements caused by the burnt edges, Fathiel used the design values from the AutoCAD software for the channel length and width in the final calculations. Channel depth is defined by the tape thickness when compressed by the cover plate. Since the tape used in this study is the same as that used in Nguyen's [35] work and the external applied forces were similar, channel depth is assumed to be the same as that reported by Nguyen. Microchannel depth measurement with a clamp and cover in place is not a trivial exercise. The laser

interferometry method proposed by Kolekar et al. [43] was applied by Nguyen for the double-sided adhesive tape channels used in this study.

Another researcher, Alshareef [34], adopted the same approach to characterize the microchannel dimensions in a xurographic counter-flow heat exchanger study. Given the study objectives for Fathiel [33] and Alshareef [34], precise channel measurements were not required.

In their reports, both Fathiel and Alshareef utilized the dimension uncertainty values determined by Nguyen [35].

Due to the difficulties associated with measuring the dimensions of a spiral microchannel produced by laser-based xurography, a decision was made to utilize the nominal channel measurements from the AutoCAD software, and the length, width, and depth uncertainty values obtained by Nguyen [35]. The three test section dimensions are shown in Table 2.2.

2.7 Uncertainty analysis

To quantify the error in the data presented herein, an uncertainty analysis was performed.

According to Moffat [38], the experimental uncertainty in an output parameter R, which is defined as a function of independent variables$x_1, x_2, \ldots, x_n$ can be determined as:

$$\delta R = \sqrt{\sum_{i=1}^{n} \left(\frac{\partial R}{\partial x_i} \delta x_i\right)^2} \tag{2.18}$$

where δR is the uncertainty value in the output parameter R, and δx_i is the uncertainty in the measured variable. Uncertainty values associated with the instruments used in the

experiment and channels dimensions are shown in Table 2.3. These data represent the x_i values when equation (2.18) was applied.

In equation (2.18) the partial derivative symbolizes the sensitivity coefficient, which may be determined analytically in some cases. When the data reduction process is more complicated, Moffat [38] proposes a numerical method using the data reduction routine where the partial derivatives are determined using a central difference approximation. This latter approach was applied in this study. The experimental uncertainty results are presented in the following section.

2.8 Results and discussion

An experimental investigation of single-phase forced convective heat transfer in heat sinks with a spiral microchannel was conducted. A set of three xurographic spiral microchannel heat sinks were fabricated, tested, and analyzed.

Four sets of tests were performed on each heat sink. Distilled water, used as the working fluid, entered the test sections at room temperature (~ 22 °C). The supplied heat ranged from 25 to 200 W and the Reynolds number ranged from 200 to 1800.

Pertinent data were extracted, saved, and analyzed. The desired outcomes in terms of the heat rate, heat flux, convection coefficient, Nusselt number, and pressure drop are presented and discussed in this section.

2.8.1 Heat rate and heat flux

During all tests performed in this investigation, the test section was well insulated. A 5 cm thick Styrofoam sheet was used to insulate all sides of the device. Holes were provided in the insulation for thermocouple and inlet/outlet ports; all were well sealed.

Tests were conducted at various power levels and mass flow rates. The time required to reach steady state ranged from 30-90 min depending on both power level and mass flow rate. In one test, steady state was reached in about 40 min, but the system kept running for an additional 90 min to ensure that the steady state status could be maintained without any significant change in measured variables. The recorded data at 40 and 130 min show that the change in variables between the two times was negligible and less than the thermocouple uncertainty, which is listed in Table 2.3.

In the initial trial for each test, the system took a long time to reach steady state, longer than subsequent trials. The device and insulation layers were at room temperature when each test started. Heating all this thermal mass to the desired temperature with a low water flow rate required a long time. Thus, it was discovered that it is not efficient to run tests at low power levels due to the long heat up time required for the system to reach steady state. One attempt was made to operate with 10 W of power provided to the heaters. In this case more than 5 hours was required for the independent variables (outlet water temperature and the eight heat sink temperatures) to stabilize and data to be recorded. In an experiment like this, to test the device at a certain power level, one thermal test is not enough to establish a relationship between a thermal parameter, such as Nusselt number, and the flow rate (in terms of the mass flow rate or Reynolds number). Thus, the device should be tested many times at different flow rates to clarify such a relationship.

A lower limit was also imposed on the mass flow rate. This limit is related to the Kapton polyimide tape; previous studies [33, 34] reported that the tape can handle temperatures up to 75°C without damage. If tape deterioration occurs, it can lead to water

leakage. Water leakage risk also imposes an upper limit on the water flow rate; it is possible that the elevated pressure inside the spiral channel that accompanies high flow rates could cause water to leak between channel walls or to the outside.

The heat rates Q for the three devices are shown in Figure 2.13 as a function of the mass flow rate $\dot{m}$. The heat gained by the water is calculated from equation (2.13) and the heat generated by the heaters is determined using equation (2.12). The first device was tested at four different power levels 25, 50, 75, and 100 W, the second was tested at 50, 100, 150, and 200 W, and the third was tested at 50, 100, 150, and 200 W, respectively.

As expected from equation (2.13), the heat transfer rate increases with increased mass flow rate for the three test sections. Figure 2.13 also shows that for the same mass flow rate and power level the three devices are almost able to extract the same amount of heat. The thermal area (A_{th}) for the three test sections is shown in Table 2.2, and as can be seen in Figure 2.13, the device with the largest thermal area is able to operate at higher flow rates and transfer more heat than the others.

Figure 2.14 presents the heat flux results for the three devices as a function of the mass flow rate, where heat flux is calculated from equation (2.14). Heat flux data have trends similar to the heat rate, where the heat flux also increases with the increase in mass flow rate. As the heat rate is almost the same for the three tested channels at the same flow and power levels, the channel with the smallest thermal area has the highest heat flux, as shown in Figure 2.14.

Results show that 44 - 70% of the power supplied to the heaters was extracted by the water and the rest was lost to the surroundings.

In general, fluid flow in a spiral channel augments the heat transfer due to the secondary flows and their mixing effects within the flow field. Thus, the thermal performance of the xurographic spiral microchannel heat sink was anticipated to be acceptable even with the use of the low thermal conductivity Kapton® tape ($k \sim 0.12$ W/m/K).

Experimental results show that even a 100μm thick layer of thermal insulating tape can form a thermal barrier that creates a significant temperature difference between the substrate and cover plate, as shown in Figure 2.15.

Figure 2.15 presents the temperature difference ΔT as a function of the mass flow rate. It is obvious that the temperature difference decreases as the mass flow rate increases, but at the same time, this difference increases with the level of the supplied power. The temperature differences observed between the substrate and cover over a short distance (5 mm) in copper are not expected. These fairly high values are due to the relatively high thermal resistance of the Kapton tape that separates the substrate and cover plate. Details about the locations of the thermocouples that were used to measure the channel wall temperature can be found in sections 2.3 and 2.4.

The heat transfer data raise a question about the unfortunate thermal performance of the tested devices and about the circumstances that could lead to such performance. Popescu et al. [39] conducted an experimental investigation on the heat transfer performance of a very shallow rectangular microchannel with aspect ratio (depth/width) ranging from 0.052 - 0.012 and Reynolds number ranging from 300 - 900. Their results showed that the very shallow channel departs significantly from macroscale predictions,

and experimental Nusselt number values were approximately 25% lower than traditional predictions.

In the experiment presented herein, the poor thermal performance could be attributed to the presence of the Kapton® tape, which has very low thermal conductivity, and to the very low channel aspect ratio (depth/width 1:10, 1:20, and 1:30, as shown in Table 2.2).

A spiral microchannel with very low aspect ratio may not have the required structure to initiate secondary flows, which are necessary to enhance thermal performance. A search in the published literature about subjects related to the flow in curved or spiraled conduits with low aspect ratio showed a scarcity of information.

2.8.2 Heat transfer coefficient and Nusselt number

The average heat transfer coefficient h is determined from equation (2.15) and presented in Figure 2.16 as a function of the mass flow rate $\dot{m}$. The data in Figure 2.16 illustrate the change in thermal performance for the three spiral channels as a function of mass flow rate and power levels. It is apparent that the change in the power level does not have much impact on the thermal behavior of the channel at the same mass flow rate, regardless of which device was tested. These data indicate a linear relationship between the average convection coefficient and flow rate; as the mass flow increases, the heat coefficient increases nearly linearly.

For a thermally and hydrodynamically fully developed laminar flow in a straight channel, the convection coefficient has a constant value along the flow path. Under similar conditions, the average heat transfer coefficient increases with the fraction of the channel that experiences developing flow. However, for flow in a spiral channel the

situation is different. The radius of curvature of a spiral channel changes along the channel length, and that change produces centrifugal forces in varying magnitude along the channel length, which makes the fully developed flow a limiting case that can be reached only when the ratio of the curvature radius to the channel radius, or the Dean number value, becomes large [40]. Therefore, from Figure 2.16 it is clear that the thermally fully developed flow condition is not achieved in the three channels. As noted previously, the channel curvature was expected to produce secondary flows, which are expected to enhance heat transfer. The secondary flows produce a turbulent flow condition, rendering the laminar flow field effects on heat transfer rates moot. For turbulent conditions, the average Nusselt number and heat transfer coefficient are dependent on the Reynolds number (or mass flow rate) and flow development length. Thus, with increasing mass flow rate and Reynolds number, *Nu* and *h* are expected to increase.

In Figure 2.17, the experimental Nusselt number *Nu* for the three spiral microchannels is presented as a function of the Reynolds number *Re*.

The experimental Nusselt number values are significantly lower than those expected in the predesign analysis (as shown in Figure 2.1). These data are also lower than results obtained in previous microchannel heat sink studies performed by other researchers [10, 29].

As explained above, this poor thermal performance may be attributed to the low thermal conductivity of Kapton® tape and the very shallow spiral microchannel. The Nusselt number is defined as the ratio of convective to conductive heat transfer rates and a Nusselt number value less than 1 indicates that the convective component is less than

the conductive part. In Figure 2.17, it can be observed that the Nusselt number for the 3 mm wide channel is greater than that for the 2 mm and 1 mm wide channels, respectively. Thus, the spiral microchannel with the wider cut section (more thermal area) shows better thermal performance than the narrower channels (less thermal area). The difference in Nusselt number that results from changing the channel width, length, or number of turns is demonstrated in Figure 2.18 as a function of the Dean number *De*. Considering Figures 2.17 and 2.18, it is evident that the Nusselt number trend with Dean number is the same as that for the Reynolds number. In both cases, it is clear that the relationship is nearly linear, and that the Nusselt number increases in value with any increase in Reynolds number or Dean number.

During the predesign, the Dravid correlation (equation 2.1) was used to predict the thermal performance of the xurographic spiral heat sink. Dravid [32] numerically studied the effect of secondary flows on laminar flow heat transfer in helically coiled tubes operating in the thermal entrance region. He proposed a correlation for the Nusselt number in terms of Dean number and Prandtl number. The Dravid correlation has been verified experimentally in the same range of flow in which the numerical study was conducted [29]. Figure 2.19 compares the Nusselt number obtained from the three test sections having different spiral channel configurations under the condition of varying Dean number and changing power levels.

Nu predicted by the Dravid correlation is much higher than that obtained in this study. In addition to the reasons previously mentioned for the low heat transfer coefficient (secondary flow suppression caused by the shallow channel dimensions and the thermal barrier associated with the Kapton tape), there are other factors that may have

contributed. In section 2.5, the heat transfer surface area was defined as the entire inner surface of the microchannel. One could also argue that the heat transfer surface area could be represented by just the bottom portion of the microchannel. Since the temperature of the microchannel cap is much lower than that of the substrate (see Figure 2.15) the heat transfer from the top portion is much less than that from the substrate. If the heat transfer surface area had been defined as others have done [10, 29] using only the lower surface, experimental h and Nu values would roughly double. The wall temperature used in the definition of h (equation (2.15)) was assumed to be equivalent to the average of the thermocouple measurements in the cap and substrate. These measurements were not made directly at the surface. It is understood that the difference in temperature between thermocouples at the same vertical location is quite small (on the order of 0.5°C). Thus, averaging temperature readings at a particular level should not introduce any significant error. It is also understood that there is some small temperature difference (again, on the order of 0.5°C) between thermocouple locations and the actual microchannel walls. By assuming the wall temperatures are equivalent to the average of the thermocouple readings within the cap and substrate, some error has been introduced. Similarly, the average fluid temperature used in the definition of h was a simple average of the inlet and outlet fluid temperatures. While it is very challenging experimentally, a better way to define the average heat transfer coefficient h is through an integrated average that takes into account local differences in the wall temperature and mean fluid temperature. This approach would lead to h data that better represent the actual experimental conditions.

2.8.3 Pressure drop

Inlet and outlet pressure measurements were made using pressure transducers located approximately 50 cm upstream and downstream from the inlet and outlet ports, respectively. It is understood that the pressure drop data from these measurements includes minor pressure losses from contractions/expansions in the four-way unions and other fittings and the connecting tubes. These pressure losses are in addition to the major pressure drop resulting from the water flow through the spiral microchannel.

The objective of presenting these pressure drop data is to estimate the energy input required to drive the flow through the device to enable the convective heat transfer processes. Figure 2.20 illustrates the total pressure drop for the three heat sinks as a function of the Reynolds number at different power levels along with pressure drop predictions for the three test sections calculated by using White correlation [22] with water properties determined at (30°C) average water temperature. White correlation [22] was explained in detail in section 2.2. Since the third device has the shortest and widest channel (as shown in Table 2.2), it is expected that it has the lowest pressure drop of the three devices at the same Reynolds number.

2.8.4 Uncertainty report

The data reduction process revealed that the largest uncertainty values were recorded during a test performed on device number three. This device has the widest channel, which permits higher flow rates and Reynolds numbers. The higher water flow rate reduces the difference between the outlet and inlet water temperatures. At the same time, the higher flow rate results in a smaller difference between the average wall temperature and the average water temperature. Since the uncertainty of the mass flow

rate is required to be below a certain value (≤ 0.1) through a condition defined in the data reduction code, the temperature measurements have the greatest impact on the uncertainty of the outputs, such as the heat rate and heat transfer coefficient.

The maximum uncertainties associated with the calculated parameters were determined according to the Moffat method [38] and are presented in Table 2.4.

2.8.5 Conclusions

An experimental study was conducted to investigate the thermal characteristics of forced convection heat transfer of distilled water flowing through a xurographic spiral microchannel heat sink. Three heat sinks with spiral microchannels having a different number of turns, lengths, widths and, hence, aspect ratios were fabricated and tested at different flow rates and power levels. The thermal behavior in terms of heat rate, heat flux, convection coefficient, and Nusselt number was calculated, presented and analyzed. Pressure drop through the system was also measured in order to evaluate the energy required to drive the flow through the heat sink producing the desired thermal processes. Unfortunately, poor thermal performance was observed. Physical explanations for the poor performance include the thermal barrier of the low thermal conductivity Kapton® tape and the use of shallow spiral microchannels, which likely suppress the formation of secondary flows. Variables used in the definition of the heat transfer coefficient have also contributed to the low h values, either by their very definition (A_{th}) or in the manner in which they were measured (T_w and T_{ave}). The Nusselt number was compared to a well-known macroscale correlation (Dravid correlation [32], for more details see section 2.2) used to describe the thermal behavior of curved channels in the laminar region.

A significant difference was observed and attributed to the poor thermal performance of the xurographic heat sink.

In general, results show that the third device has the best thermal performance with the least required driving pressure, as shown in Figures 2.17 and 2.20. However, further investigation is required to better utilize the heat transfer enhancement of the secondary flows associated with the spiral channel pattern along with the xurographic fabrication technique.

Table 2.1 Dimensions of the three microchannels used in the analytical model

Channel No.	Width (mm)	Height (mm)	Length (mm)	Aspect Ratio	No. Spirals
1	0.5	0.105	320	0.21	4.375
2	1	0.105	255	0.105	3.375
3	2	0.105	185	0.0525	2.375

Table 2.2 Geometrical parameters of the test sections

Test section #	W_c (mm)	H* (mm)	L (mm)	D_h (mm)	W_p (mm)	D_r (mm)	γ	No. of Spirals
1	1	0.105	351.746	0.1900	3	2	0.105	4.5
2	2	0.105	279.667	0.1995	3	3	0.0525	3.5
3	3	0.105	210.984	0.2028	4	3	0.035	2.5

*In this study, channel depth was assumed to be equal to the tape thickness measured by Nguyen [35] as long as the same force was applied to the clamping system with the same bolt torque sequence.

Table 2.3 Uncertainties in the measured data

Measurement	Unit	Uncertainty
Thermocouple	°C	±0.5
Setra Pressure Sensor	psi	±0.15% of full scale
Mass Balance	g	±0.01
LabView Internal Clock	s	±0.01
Voltmeter	V	0.16% ± 30 mV
Channel Length*	μm	±1.0
Channel Width*	μm	±1.0
Channel Depth*	μm	±0.5

* Dimension uncertainties as characterized by Nguyen [35] were used in this study.

Table 2.4 Maximum relative uncertainties associated with the key outputs

Parameter	*Re*	*Q*	*q*	*h*	*Nu*	*De*
Max. Relative uncertainty %	0.82	9.85	9.85	11.46	11.43	0.84

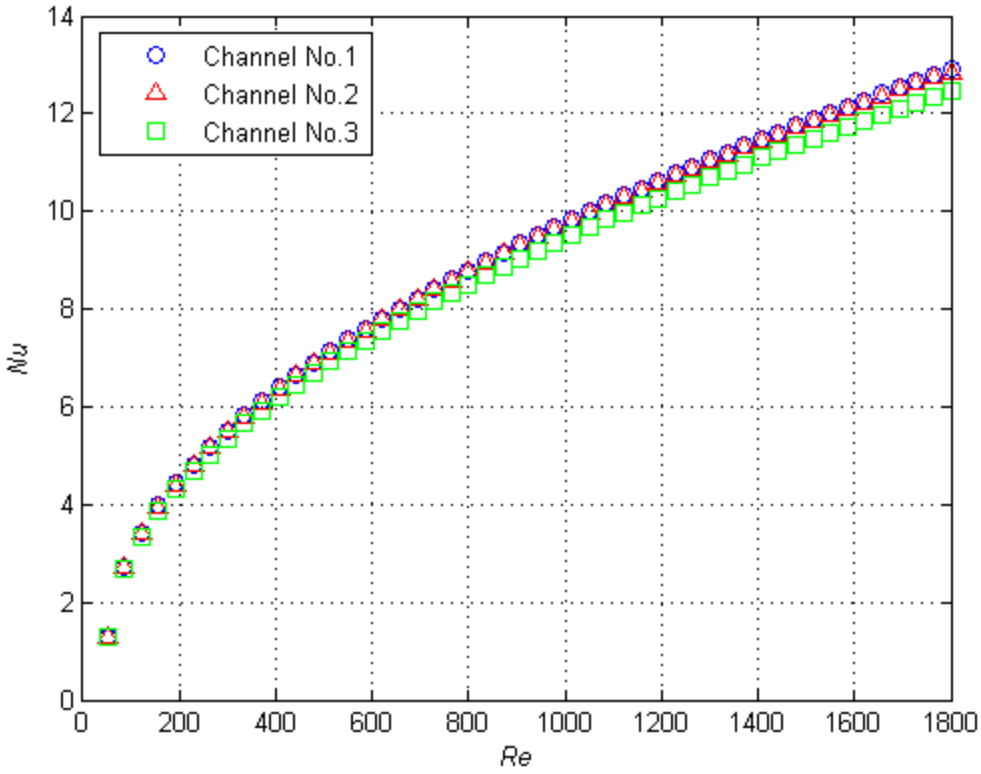

Figure 2.1 Predicted thermal performance of the three microchannels

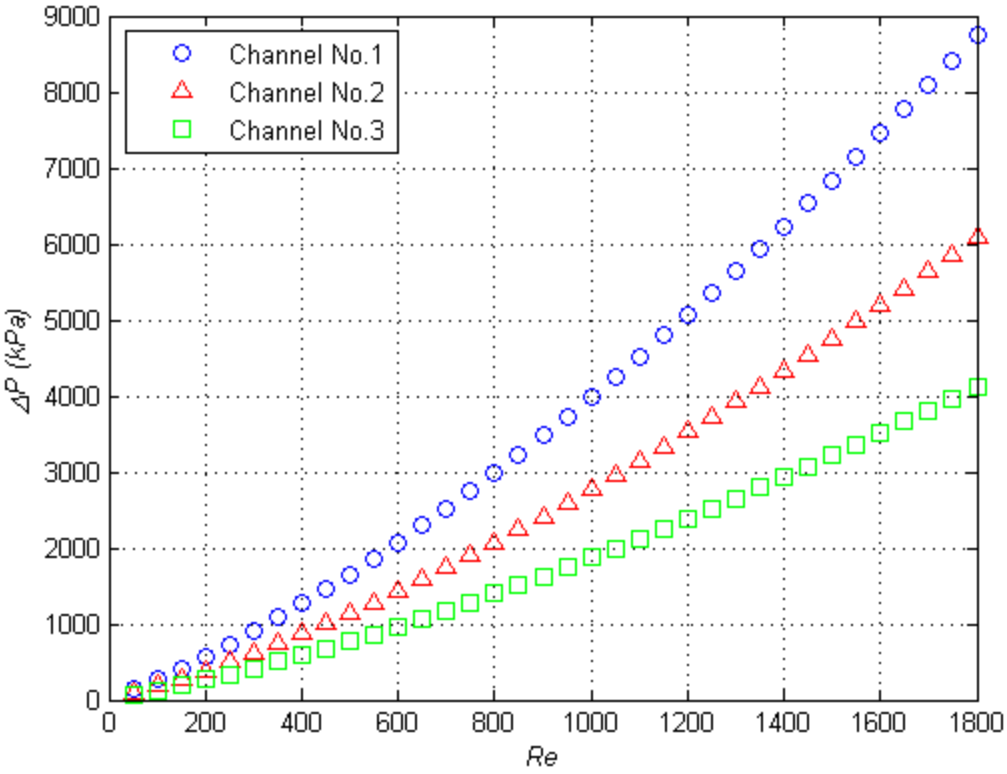

Figure 2.2 Predicted pressure drop for three microchannels

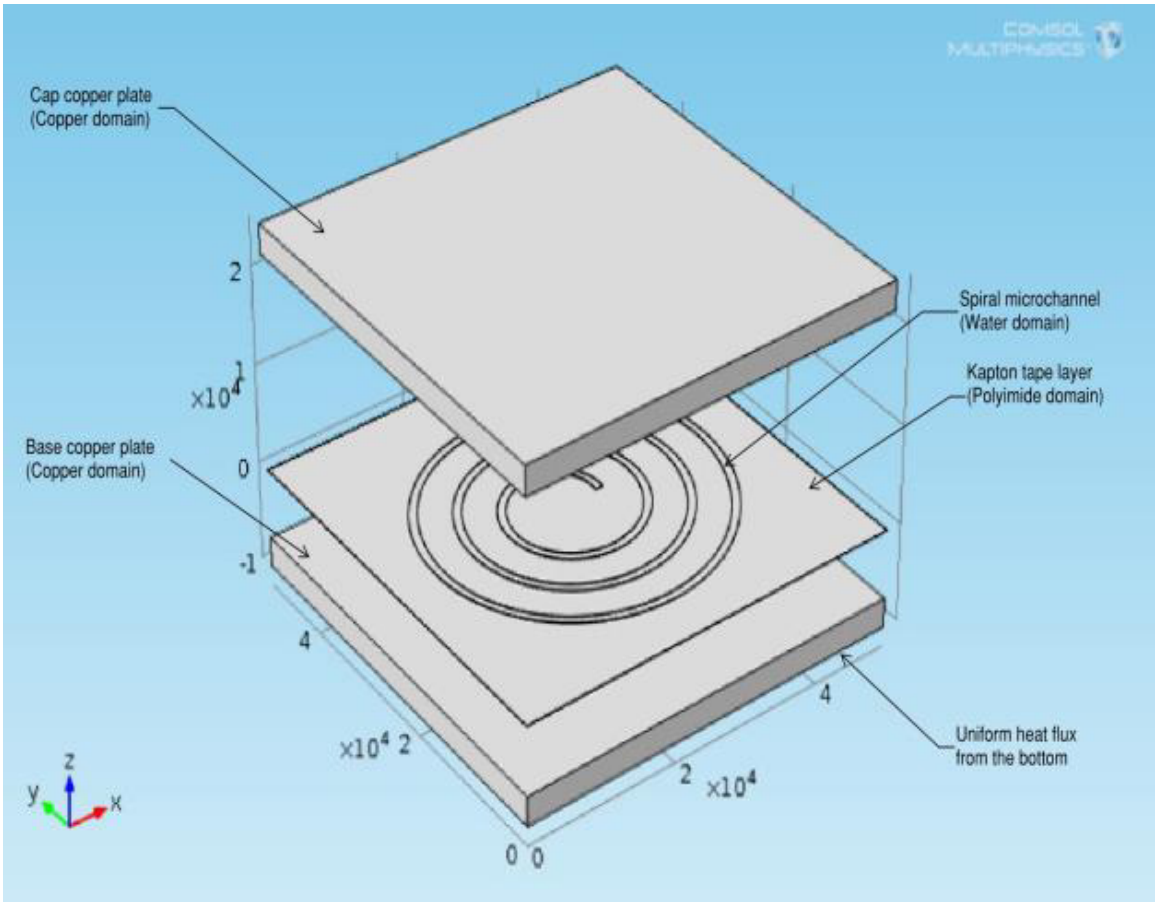

Figure 2.3 Schematic of the three-dimensional COMSOL model for the xurographic spiral microchannel heat sink. Dimensions are in cm.

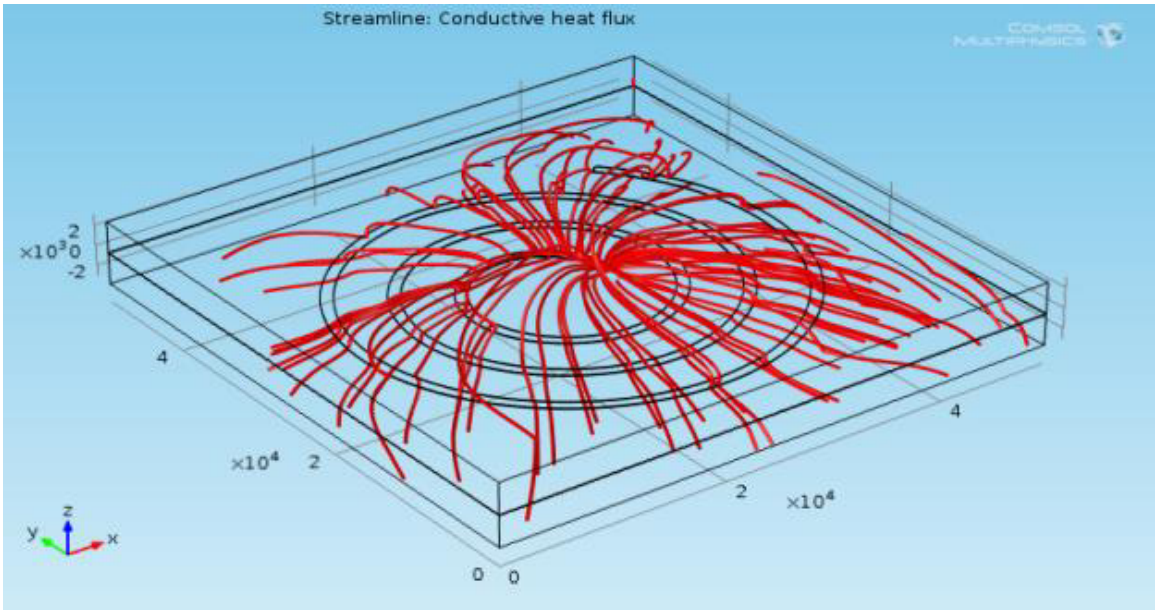

Figure 2.4 Streamlines for the conductive heat flux from the COMSOL model

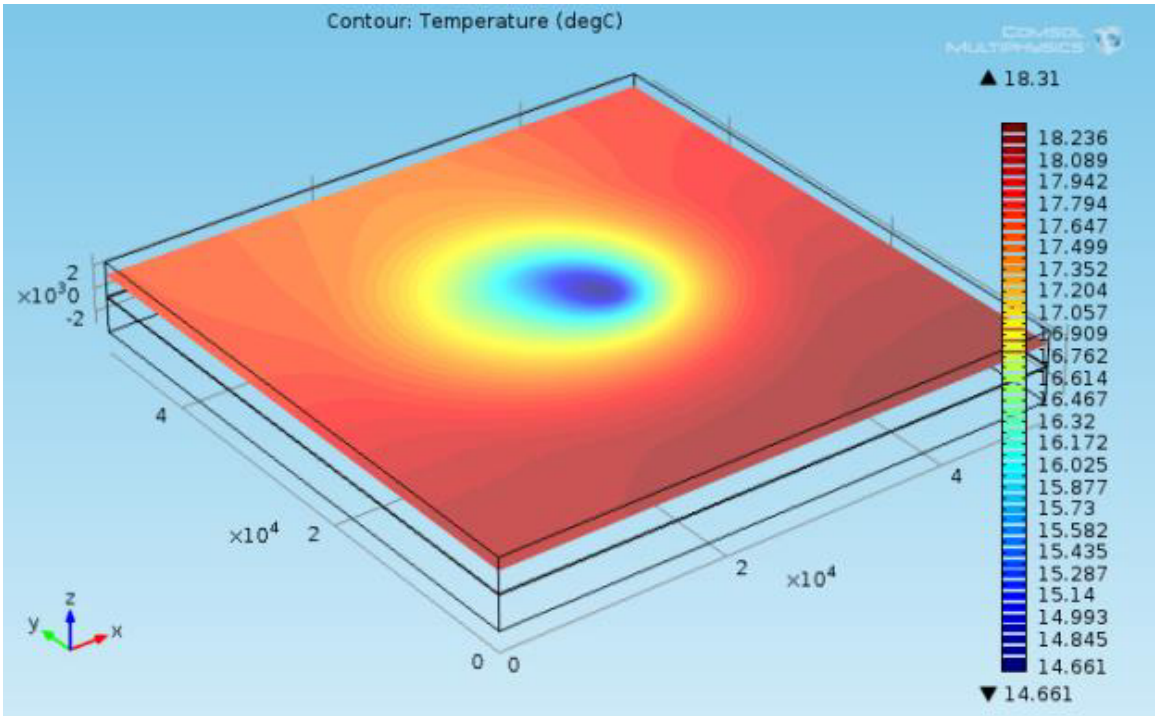

Figure 2.5 Temperature contours for a surface 2 mm above the channel

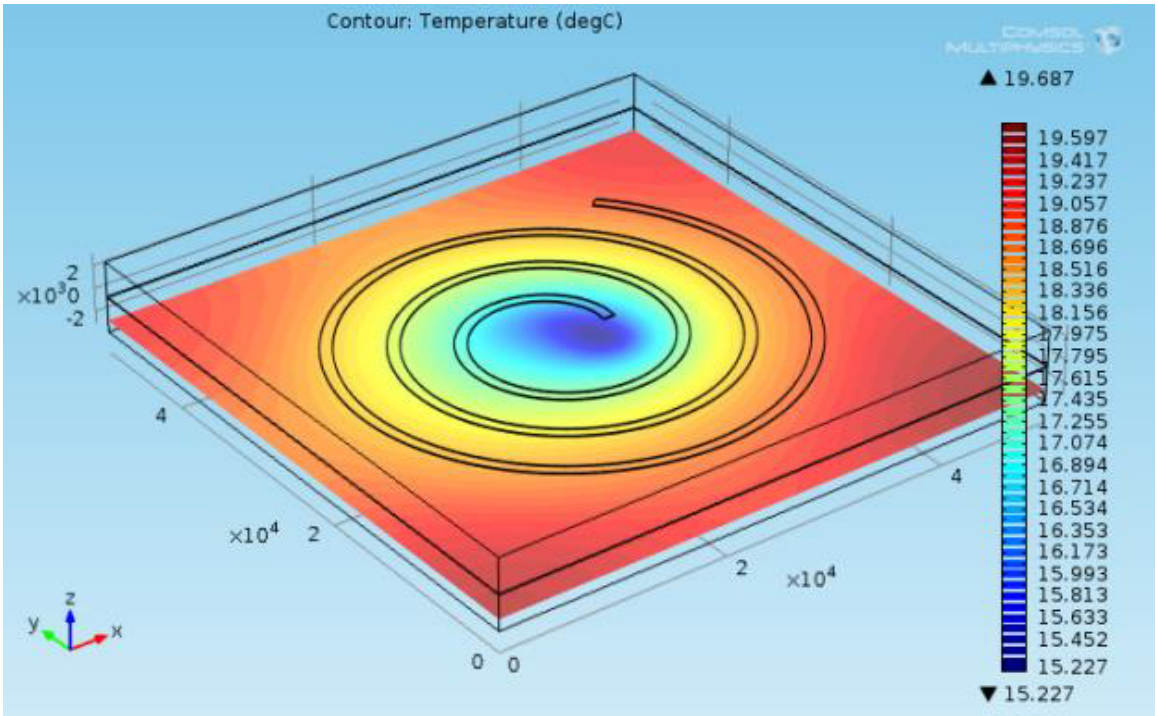

Figure 2.6 Temperature contours for a surface 2 mm below the channel

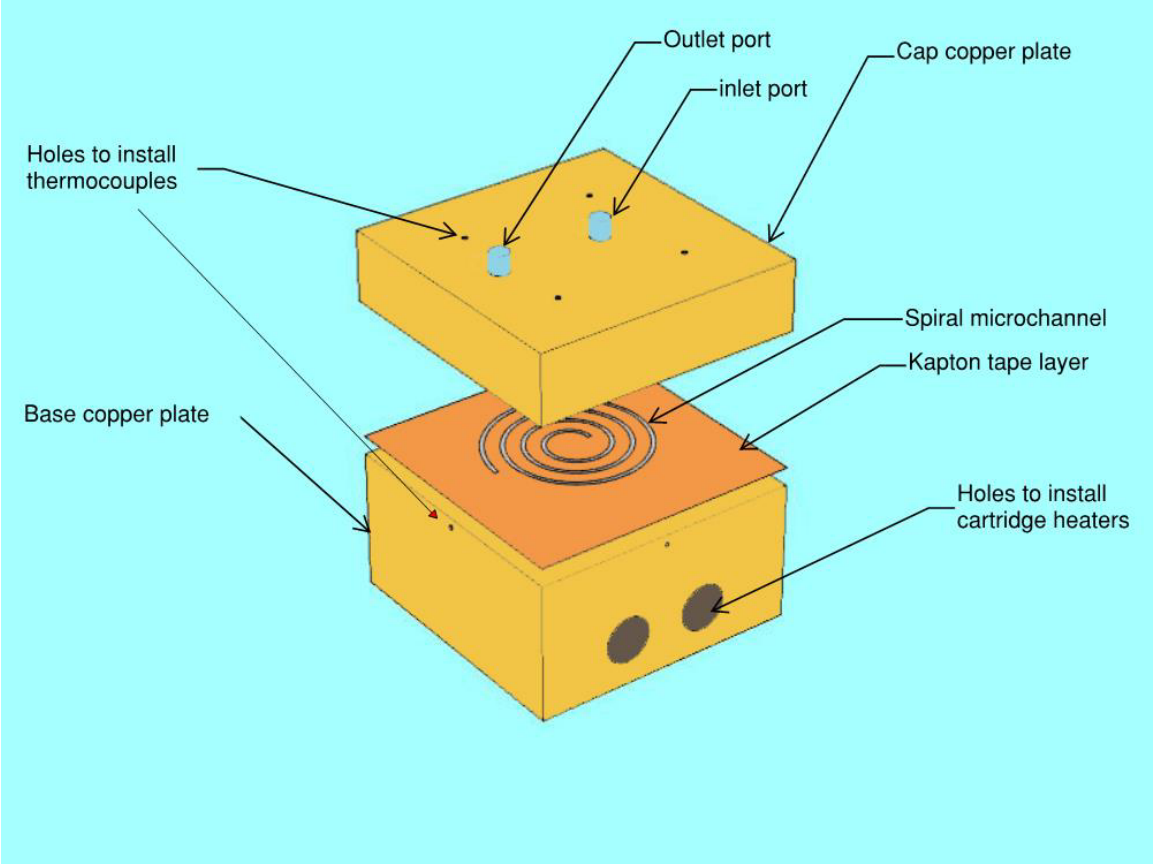

Figure 2.7 Schematic details of the heat sink three-dimensional assembly diagram

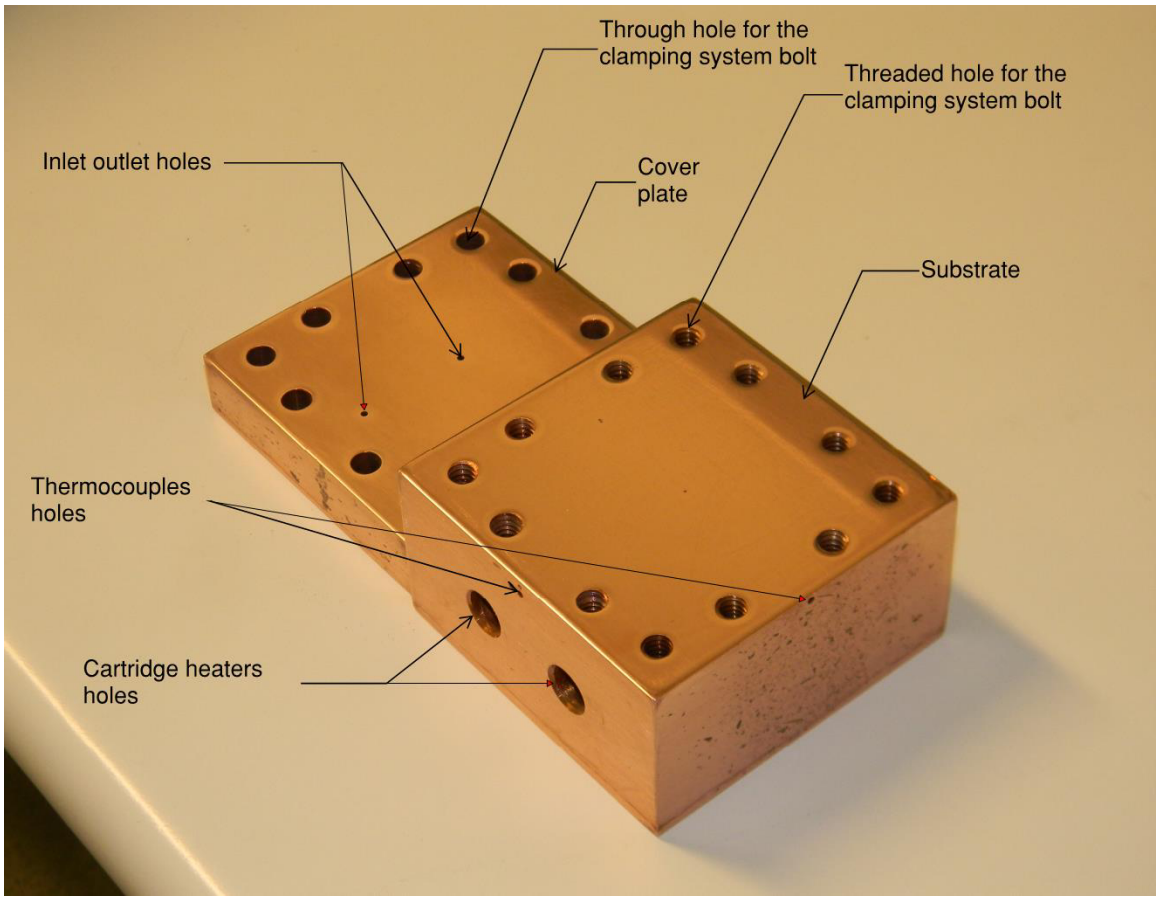

Figure 2.8 Photograph of the two machined and polished copper pieces

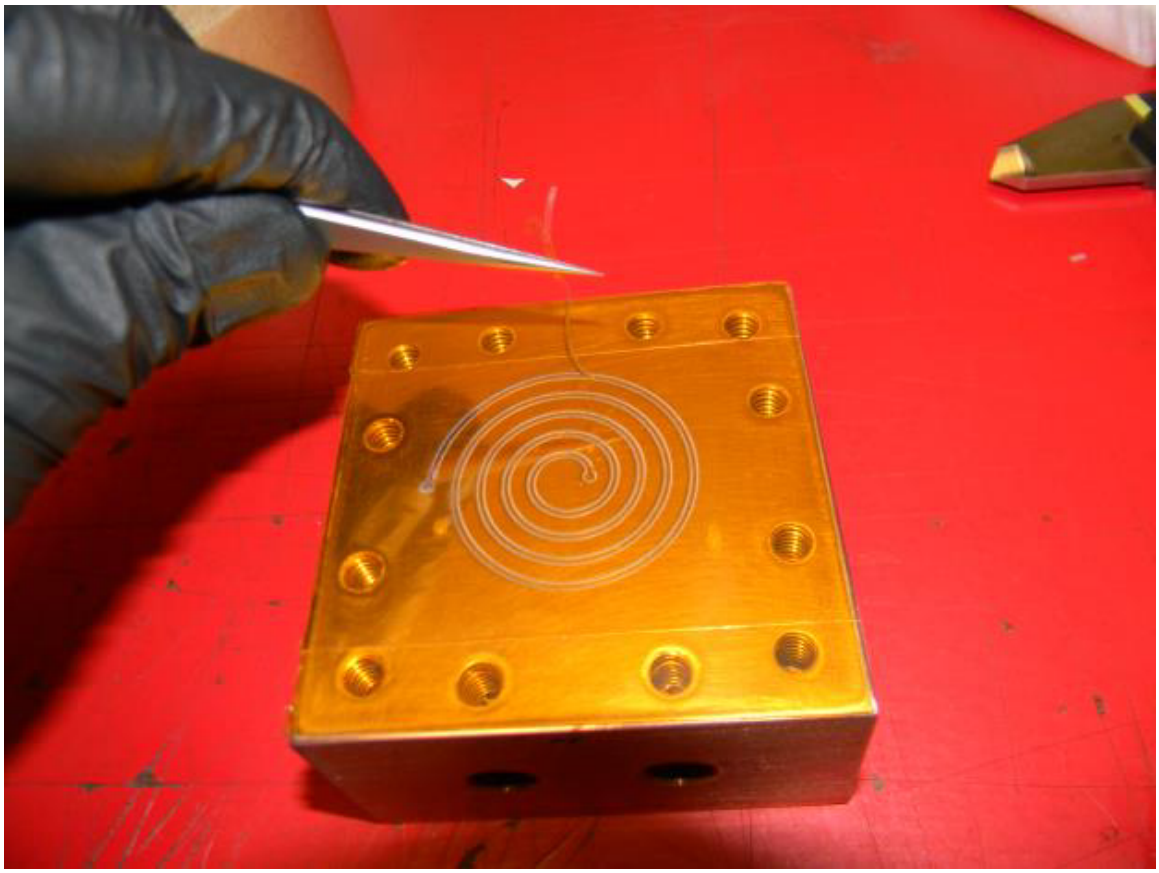

Figure 2.9 Photograph of cut spiral channel in the Kapton® tape on the substrate

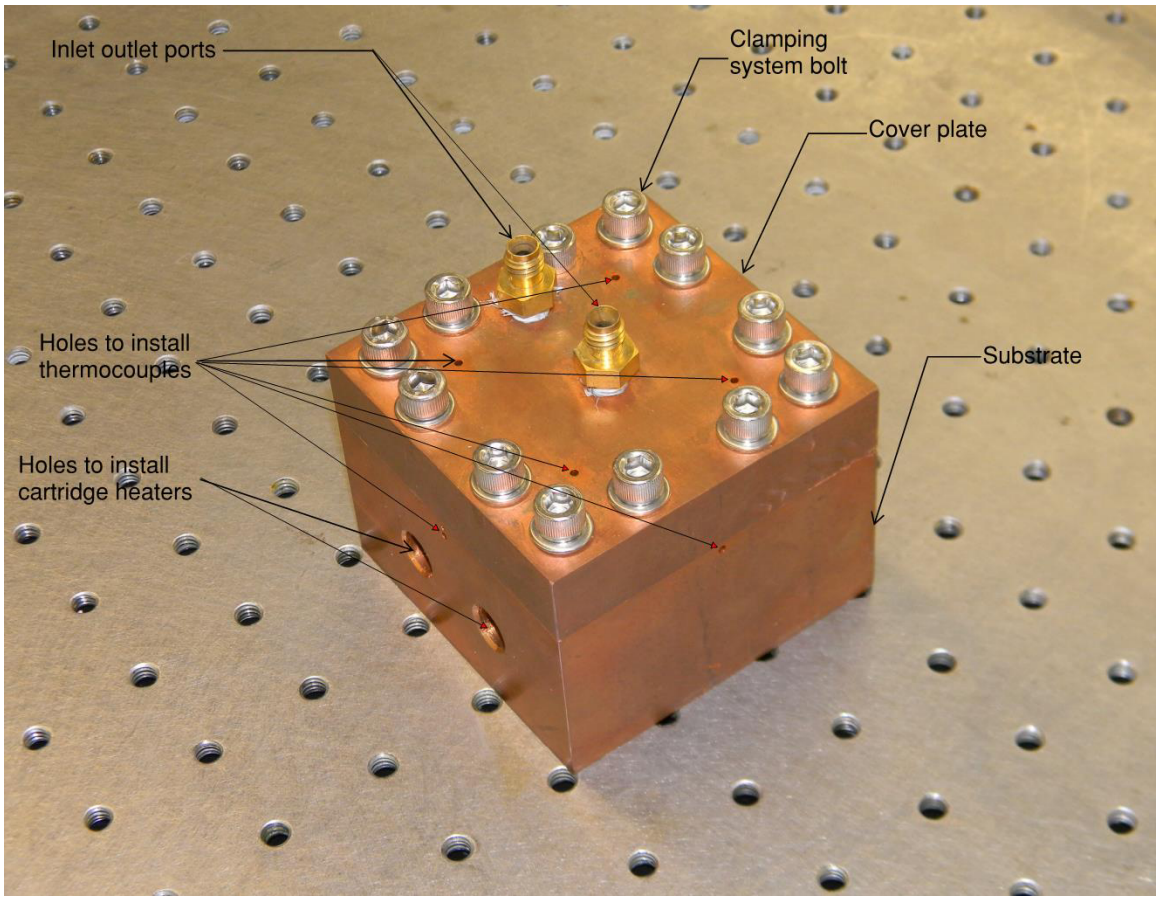

Figure 2.10 Photograph of the final assembled device

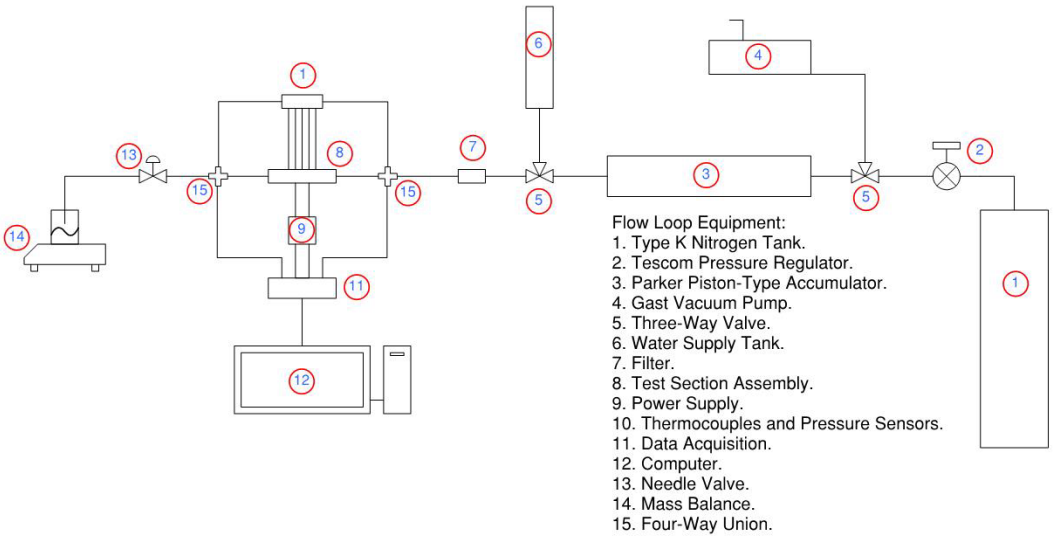

Figure 2.11 Schematic of the experimental flow loop

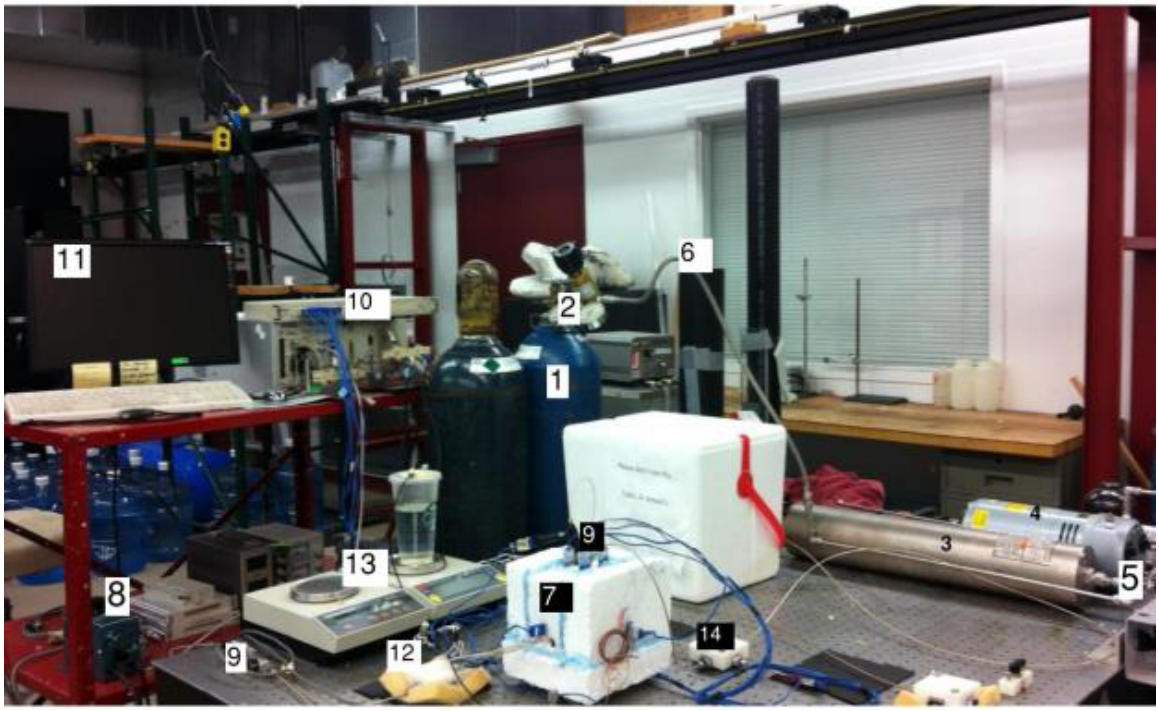

Figure 2.12 Photograph of the test loop. (1) Nitrogen tank, (2) pressure regulator, (3) accumulator, (4) vacuum pump, (5) three-way valve, (6) water tank, (7) test section, (8) power supply, (9) thermocouples and pressure sensors, (10) data acquisition system (11) computer, (12) needle valve, (13) mass balance, (14) four-way union.

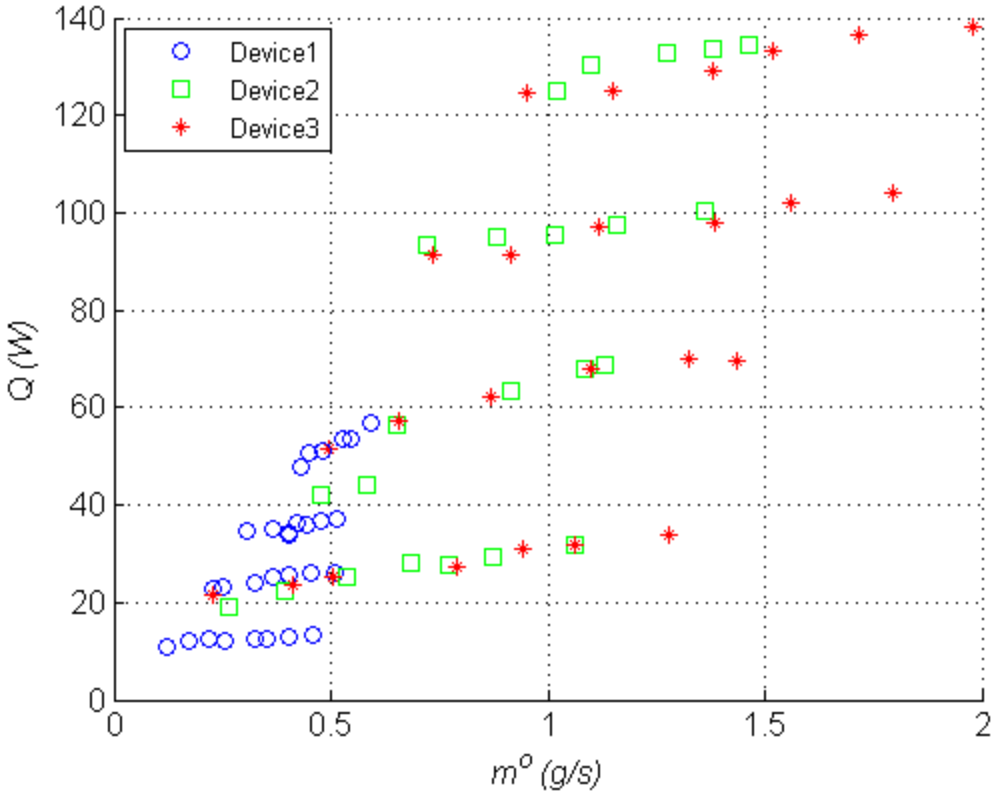

Figure 2.13 Effect of mass flow rate on the heat rate for the three test sections at different power levels

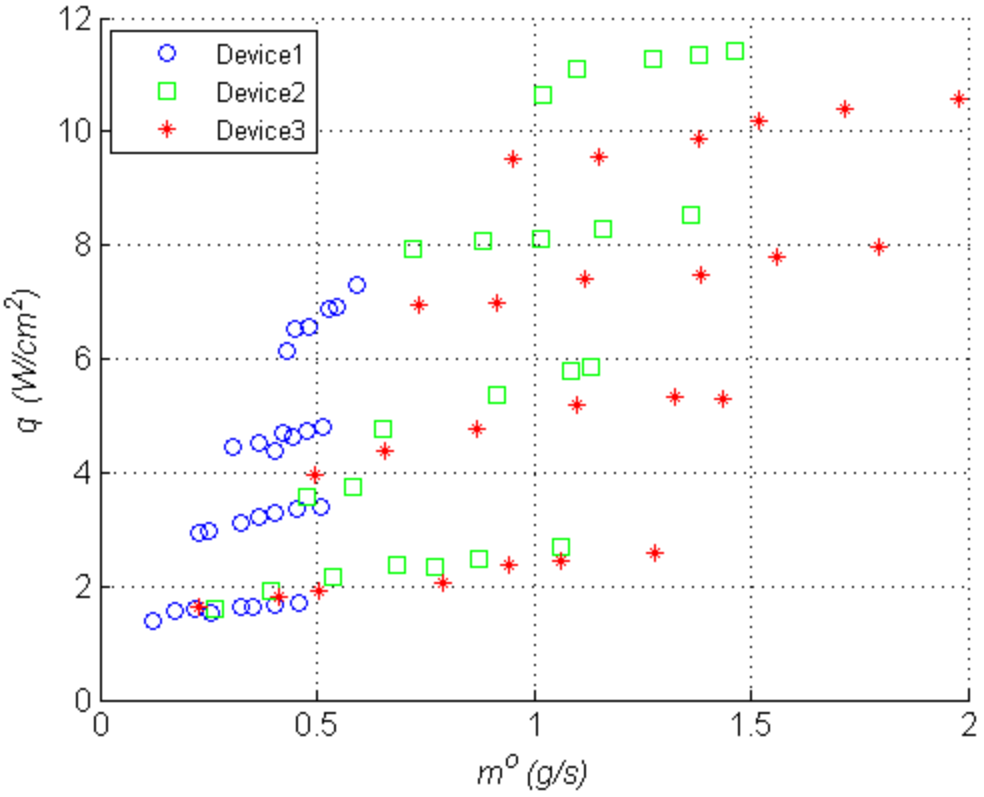

Figure 2.14 Effect of mass flow rate on the heat flux for the three test sections at different power levels

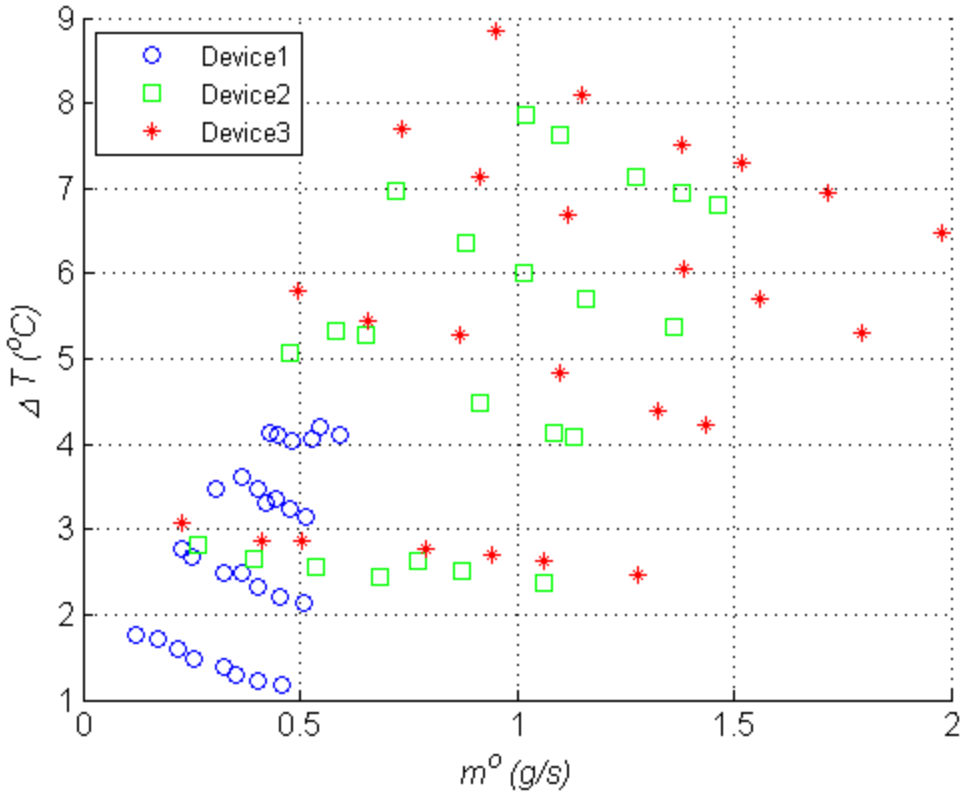

Figure 2.15 Effect of mass flow rate on the temperature difference between the upper and lower copper blocks for the three test sections at different power levels

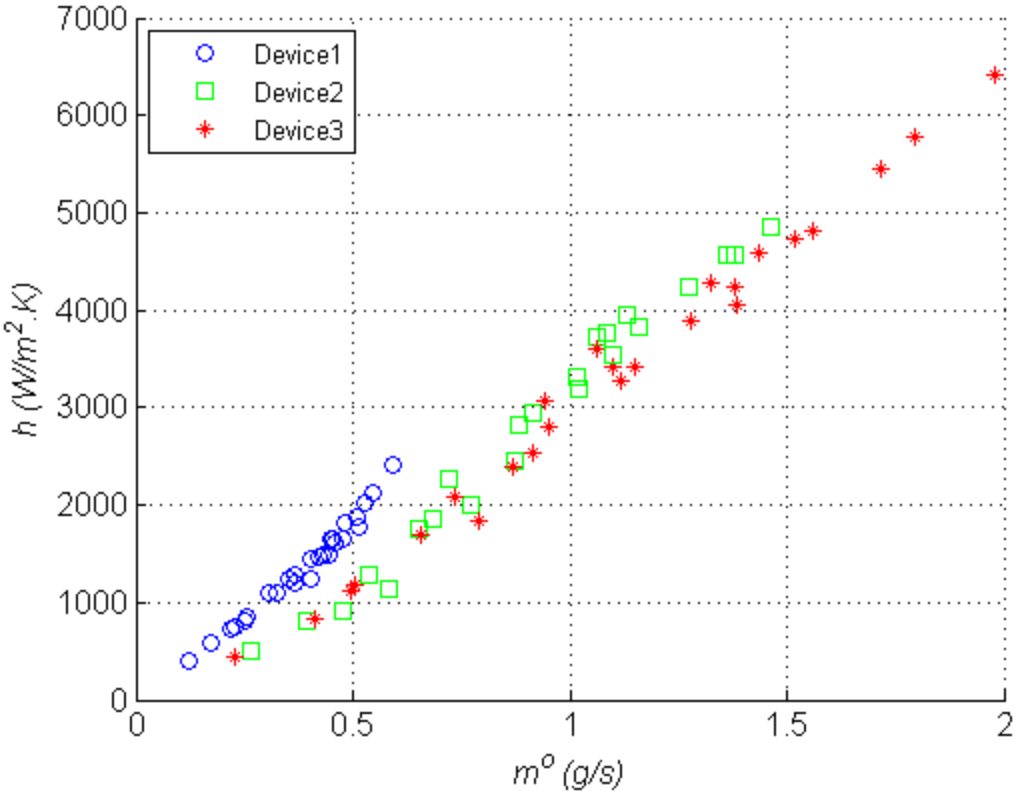

Figure 2.16 Effect of the mass flow rate on the heat coefficient for the three test sections at different power levels

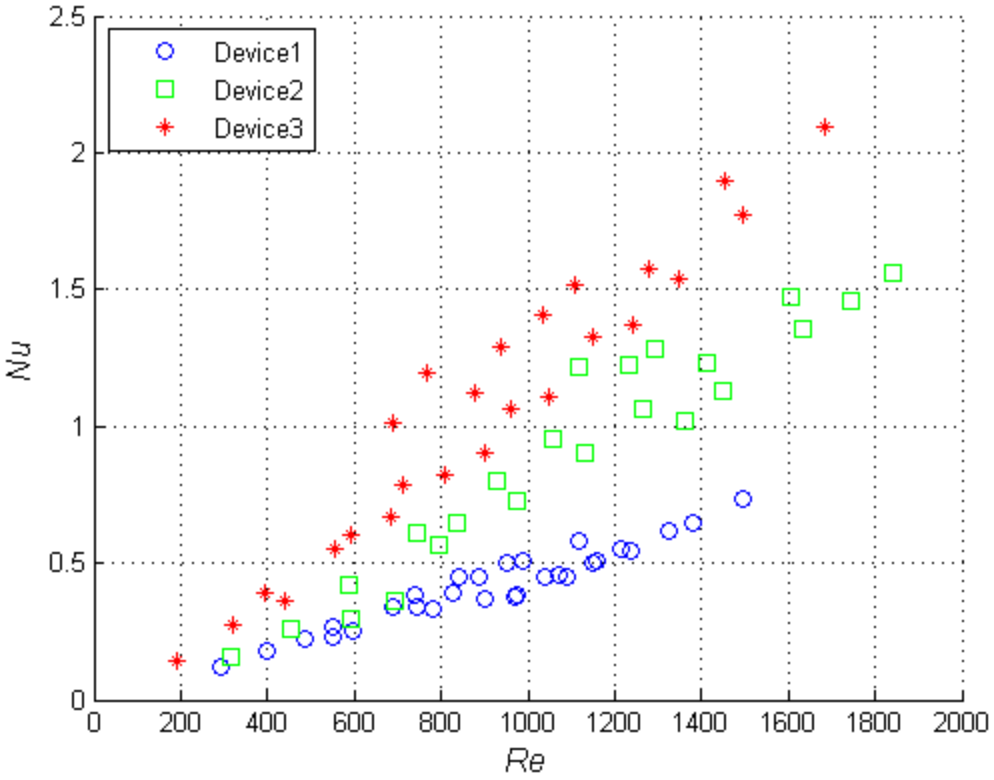

Figure 2.17 Nusselt number as a function of Reynolds number for the three test sections at different power levels

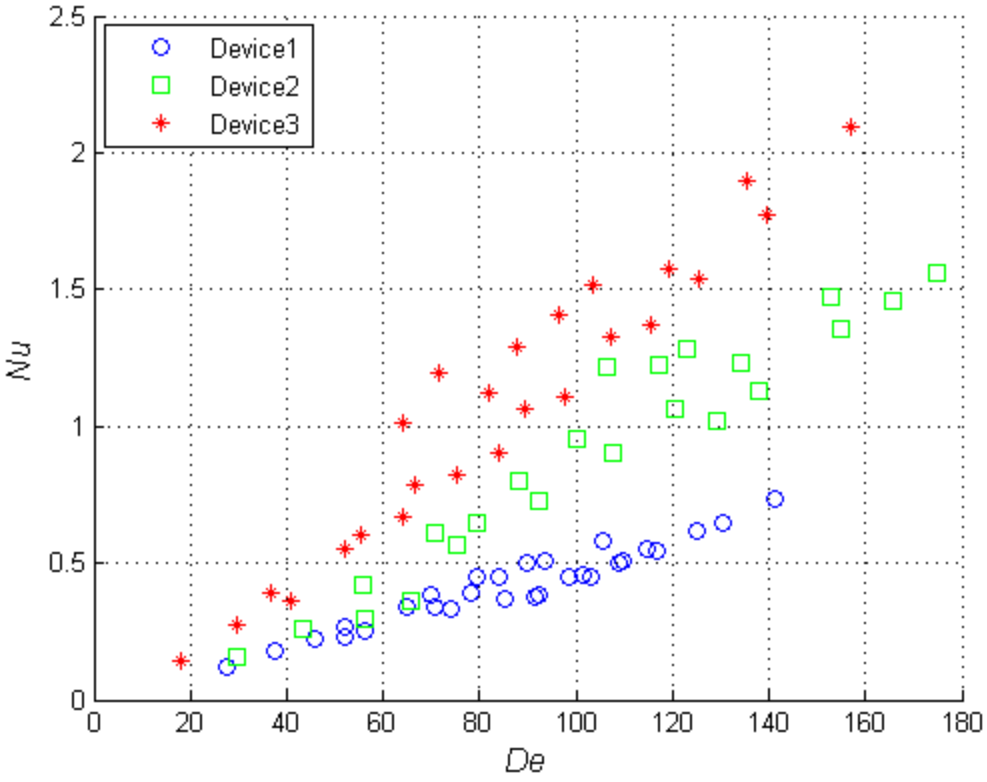

Figure 2.18 Nusselt number as a function of Dean number for the three test sections at different power levels

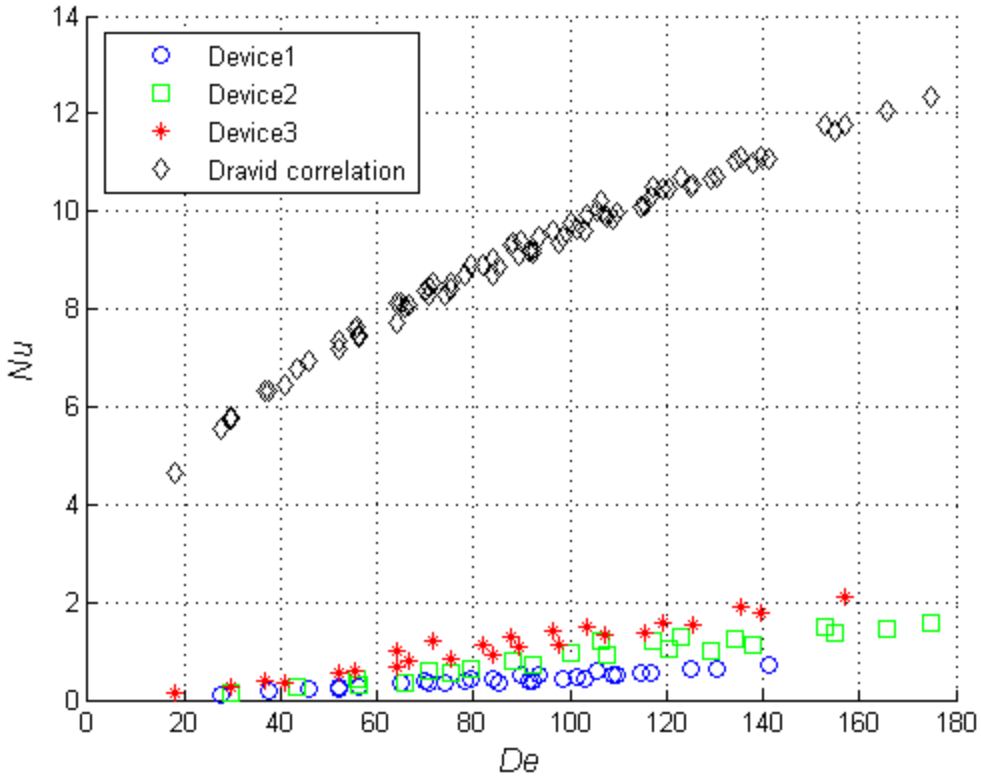

Figure 2.19 Comparison of the experimental Nusselt number to that predicted from the Dravid correlation [32]

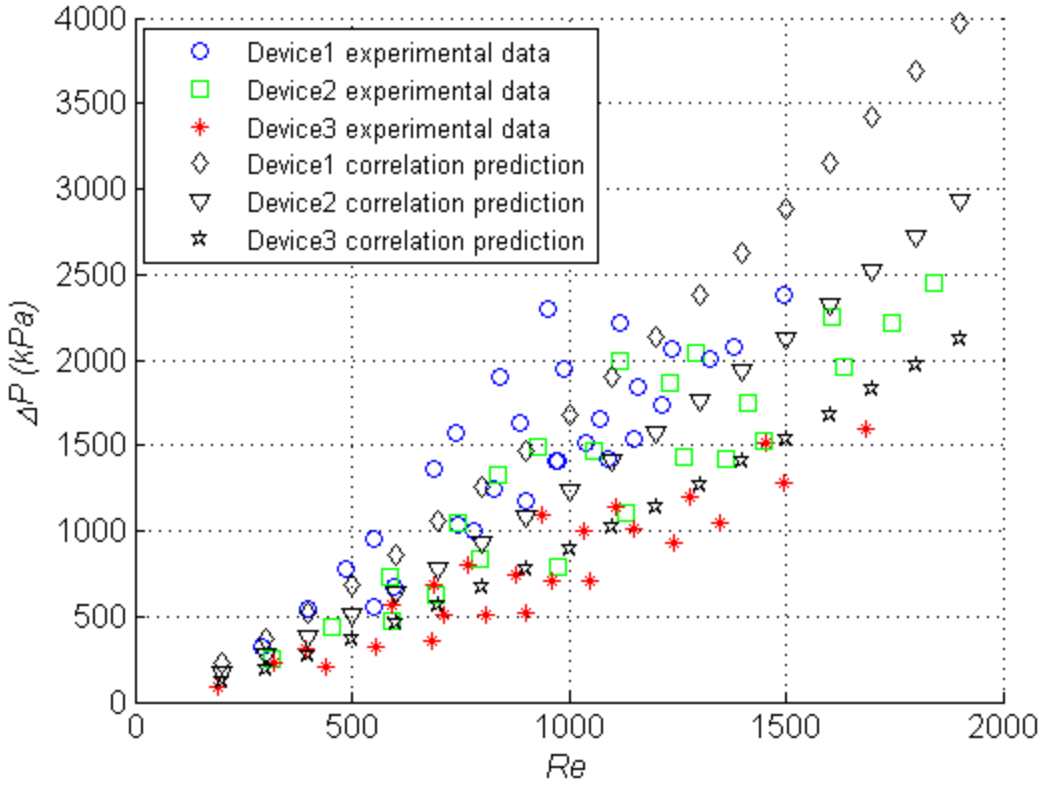

Figure 2.20 Experimental pressure drop as a function of Reynolds number for the three test sections at different power levels compared to macroscale prediction

2.9 References

[1] D. A. Bartholomeusz, R. W. Boutte, J. D. Andrade, Xurography: rapid prototyping of microstructures using a cutting plotter, Journal of Microelectromechanical Systems 14 (2005) 1364-1374.

[2] D. B. Tuckerman, R. F. W. Pease, High-performance heat sinking for VLSI, IEEE Electron Device Letters 2 (1981) 126-129.

[3] P. Y. Wu, W. A. Little, Measurment of the heat transfer characteristics of gas flow in fine channel heat exchangers for microminiature refrigerators, Cryogenics 24 (1984) 415-420.

[4] J. Pfahler, J. Harley, H. Bau, J. Zemel, Liquid transport in micron and submicron channels, Sensors Actuators A: Physical 22, (1989) 431-434.

[5] X. F. Peng, B. X. Wang, G. P. Peterson, H. B. MA, Experimental investigation of heat transfer in flat plates with rectangular microchannels, International Journal of Heat and Mass Transfer 38 (1995) 127-137.

[6] X. F. Peng, G. P. Peterson, The effect of thermofluid and geometrical parameters on convection of liquid through rectangular microchannels, International Journal of Heat and Mass Transfer 38 (1995) 755-758.

[7] X. F. Peng, G. P. Peterson, Convective heat transfer and flow friction for water flow in microchannel structures, International Journal of Heat and Mass Transfer 39 (1996) 2599-2608.

[8] C. B. Sobhan, S. V. Garimella, A comparative analysis of studies on heat transfer and fluid flow in microchannels, Microscale Thermophysical Engineering 5 (2001) 293-311.

[9] G. L. Morini, Single-phase convective heat transfer in microchannels: a review of experimental results, International Journal of Thermal Sciences 43 (2004) 631-651.

[10] P. S. Lee, S. V. Garimella, D. Liu, Investigation of heat transfer in rectangular microchannels, International Journal of Heat and Mass Transfer 48 (2005) 1688-1704.

[11] W. Owhaib, B. Palm, Experimental investigation of single-phase convective heat transfer in circular microchannels, Experimental Thermal and Fluid Science 28 (2004) 105-110.

[12] W. Qu, I. Mudawar, Analysis of three-dimensional heat transfer in microchannel heat sinks, International Journal of Heat and Mass Transfer 45 (2002) 3973-3985.

[13] G. Gamrat, M. F. Marinet, D. Asendrych, Conduction and entrance effects on laminar liquid flow and heat transfer in rectangular microchannels, International Journal of Heat and Mass Transfer 48 (2005) 2943-2954.

[14] P. Naphon, S. Wongwises, A review of flow and heat transfer characteristics in curved tubes, Renewable and Sustainable Energy Reviews 10 (2006) 463-490.

[15] Y. Fan, I. Hassan, Investigation of cooling performance of a swirl microchannel heat sink by numerical simulation, Proceedings of the Ninth ASME International Conference, ASME, Alberta, Canada, 2011, pp. 1-7.

[16] Y. Wang, G. F. Ding, Experimental investigation of heat transfer performance for a novel microchannel heat sink, Journal of Micromechanics and Microengineering 18 (2008) 1-8.

[17] D. Heymann, D. Pence, V. Narayanan, Optimization of fractal-like branching microchannel heat sinks for single-phase flows, International Journal of Thermal Sciences 49 (2010) 1383-1393.

[18] H. A. Mohammed, P. Gunnasegaran, N. H. Shuaib, Influence of channel shape on the thermal and hydraulic performance of microchannel heat sink, Inernational Communications in Heat and Mass Transfer 38 (2011) 474-480.

[19] C. Liu, J. T. Teng, J. C. Chu, Y. L. Chiu, S. Huang, S. Jin, T. Dang, R. Greif, H. H. Pan, Experimental investigation on liquid flow and heat transfer in rectangular microchannel with longitudinal vortex generators, International Journal of Heat and Mass Transfer 54 (2011) 3069-3080.

[20] W. R. Dean, Note on the motion of fluid in a curved pipe, The London, Edinburgh and Dublin Philosophical Magazine and Journal of Science 4 (1927) 208-233.

[21] W. R. Dean, The streamline motion of fluid in a curved pipe, The London, Edinburgh and Dublin Philosophical Magazine and Journal of Science 5 (1928) 673-695.

[22] C. M. White, Streamline flow through curved pipes, Proceeding of the Royal Society of London, Series A Mathematical and Physical Science 123 (1929) 645-695.

[23] S. Thangam, N. Hur, Laminar secondary flows in curved rectangular ducts, Journal of Fluid Mechanics, 217 (1990) 421-440.

[24] R. S. Downing, G. Kojasoy, Single and two-phase pressure drop characteristics in miniature helical channels, Experimental Thermal and Fluid Science 26 (2002) 535-546.

[25] P. Naphon, S. Wongwises, A study of the heat transfer characteristics of a compact spiral coil heat exchanger under wet-surface conditions, Experimental Thermal and Fluid Science 29 (2005) 511-521.

[26] W. Yang, J. Zhang, H. Cheng, The study of flow characteristics of curved microchannel, Applied Thermal Engineering 25 (2005) 1894-1907.

[27] J. Chu, J. Teng, R. Greif, Experimental and numerical study on the flow characteristics in curved rectangular microchannels, Applied Thermal Engineering 30 (2010) 1558-1566.

[28] J. Chu, J. Teng, T. Xu, S. Huang, S. Jin, X. Yu, T. Dang, C. Zhang, R. Greif, Characterization of frictional pressure drop of liquid flow through curved rectangular microchannels, Experimental Thermal and Fluid Science 38 (2012) 171-183.

[29] Y. Xi, J. Yu, Y. Xie, H. Gao, Sinle-phase flow and heat transfer in swirl microchannels, Experimental Thermal and Fluid Science 34 (2010) 1309-1315.

[30] M. Ghobadi, and Y. S. Muzychka, Heat transfer in spiral channel heat sinks, Proceedings of the Ninth ASME International Conference, ASME, Alberta, Canda, 2011, pp. 1-9.

[31] R. C. Weast, 1988, CRC Handbook of Chemistry and Physics, First ed., CRC Press, Boca Raton, Florida, 1988.

[32] A. N. Dravid, K. A. Smith, E. W. Merill, P. L. Brain, Effect of secondary fluid motion on laminar flow heat transfer in helically coiled tubes, AIChE Journal 17 (1971) 1114-1122.

[33] F. A. Fathiel, Microscale cross-flow heat exchanger fabricated by laser-based xurography, MS thesis, University of Utah, Salt Lake City, UT, 2012.

[34] S. M. Alshareef, Experimental study of xurographic microchannel single-pass single-phase counterflow heat exchanger, MS thesis, University of Utah, Salt Lake City, UT, 2012.

[35] L. Nguyen, Contraction/expansion effects in 90° miter bends in rectangular xurographic micro-channels, MS thesis, University of Utah, Salt Lake City, UT, 2011.

[36] D, Torgerson, Microscale loss coefficients through expansion and contraction xurographic microchannels, MS thesis, University of Utah, Salt Lake City, UT, 2010.

[37] R. Kolekar, Fluid flow characteristics in xurographic microchannels, MS thesis, University of Utah, Salt Lake City, UT, 2009.

[38] R. J. Moffat, Describing the uncertainties in experimental results, Experimental Thermal and Fluid Science 1 (1988) 3-17.

[39] A. Popescu, J. R. Welty, D. Pfund, D. Rector, Thermal measurement in rectangular microchannels, Proceedings of IMECE International Mechanical Engineering Congress and Exposition, ASME, New Orleans, Louisiana, 2002, pp. 277-284.

[40] S. Kakac, R. K. Shah, W. Aung, Handbook of single-phase convective heat transfer, First ed., Wiley, New York, 1987.

[41] R. K. Shah, and A. L. London, Laminar flow forced convection in ducts: a sourcebook for compact heat exchanger analytical data, First ed., Academic Press, New York, 1978.

[42] R. Kalaivanan, and R. Rathnasamy, Experimental investigation of forced convective heat transfer in rectangular microchannels, ARPN Journal of Engineering and Applied Sciences 5 (2010) 21-26.

[43] R. Kolekar, R. Torgerson, D. Viner, B. J. Gale, T. Ameel, Depth measurement in fully-enclosed microchannels using laser interferometry, Measurement Science and Technology 23 (2012) 1-5.

CHAPTER 3

CONCLUSIONS AND RECOMMENDATIONS

3.1 Conclusions

Xurography has been identified as a rapid prototyping micromanufacturing technology that, in contrast with the expensive and time consuming traditional microfabrication technologies enables the fabrication of inexpensive microfluidic devices in a short time frame. In this study, xurographic spiral microchannel heat sinks were successfully fabricated and tested. The single-phase forced convection heat transfer characteristics for distilled water in xurographic spiral microchannel heat sinks were investigated at different flow rates and heat fluxes. The heat sinks were constructed using a laser-based xurographic technology, in which the spiral pattern was cut in double-sided adhesive Kapton® tape, which has a total thickness of approximately 105 μm; the cut section was removed and soot produced by laser heating was rinsed away with water. The remaining portion of the tape forms a spiral channel between two copper plates. The two copper blocks also formed an external mechanical clamping system, which applied an additional well-distributed force to the test section to minimize the potential risk of leakage. Three different heat sinks were fabricated with nominal channel widths of 1 mm, 2 mm, and 3 mm, respectively, and nominal channel lengths of 352 mm, 280 mm, and 210 mm, respectively. The channel depth was fixed by the tape thickness; thus, changes

to channel hydraulic diameter and aspect ratio were created by alterations to the channel width. Four sets of tests were performed on each heat sink, with the distilled water entering the test section at room temperature (~ 22 °C). The heat provided by cartridge heaters ranged from 25 to 200 W, and the Reynolds number ranged from 200 to 1800. Due to the high pressure requirements and the limited flow capacity of the test system, traditional turbulent flow was not considered in this investigation. On the other hand, expected secondary flows resulting from channel curvature may have produced turbulent conditions. Mass flow rate relative uncertainty was kept low (≤ 0.1%) in order to minimize the relative uncertainty of the desired outcomes. All independent variables were measured, extracted, saved, and analyzed, and the desired outcomes in terms of the heat rate, heat flux, heat transfer coefficient, Nusselt number, and pressure drop were presented and discussed. Results showed that for the same mass flow rate and power level, all three devices extracted nearly the same amount of heat. The widest channel (3 mm) was found to be capable of transferring 140 W of heat to the coolant, which represents the highest heat rate in the study. The heat rate was found to increase with the heat transfer area A_{th}. The three devices extracted nearly the same amount of heat at the same flow rate. Therefore, the heat flux was found to increase with decreased heat transfer area A_{th}. Since the third test section has the shortest and widest channel, the pressure drop for this device was the lowest for the same Reynolds number. Considering all the tests, the heat transfer coefficient ranged from 400 to 6500 W/m²/K, and the Nusselt number ranged from 0.12 to 2.1. The experimentally obtained Nusselt number was compared to a macroscale prediction from the Dravid correlation. Comparisons showed that the Nusselt number computed using Dravid correlation is much higher than

that found in this study. This significant deviation reflects the disappointing thermal performance of the xurographic spiral microchannel heat sink. However, measurement limitations (primarily wall and fluid temperatures) and differences in definitions (primarily, heat transfer surface area) produced results that are better than they first appear. It is evident that xurography can be used to produce a spiral microchannel heat sink in a simple and inexpensive way; however, the low thermal conductivity Kapton® tape diminishes the thermal performance of such a device.

Answers to the questions presented in the first chapter can now be determined and are presented here:

- Using xurographic technology, a spiral microchannel heat sink can be fabricated with double-sided adhesive Kapton® tape and copper plates. Unfortunately, the thermal performance of such devices was found to be less than desired.
- The maximum operating wall temperature achieved without water leakage or failure was 79°C. The maximum inlet pressure for the heat sinks without water leakage or failure was 2500 kPa.
- The spiral microchannels produced by the laser cutting system were found to be more precise than those produced using the blade cutting system. The laser cutting process creates soot and burns on the channel walls. The soot and burnt material prevents precise measurement of microchannel dimensions.
- The smallest channel width achieved in this study was 1 mm.
- The maximum heat rate dissipated in this experiment was approximately 140 W.

- No significant difference in thermal performance was found between the three test sections as a result of changes to geometric design.

3.2 Recommendations

Several recommendations can be proposed to improve the current study if it were to be repeated. These enhancements are in the general areas of the fabrication process, test procedure controllability, and result accuracy.

- Due to the soot and burned edges produced by the laser heating, it is recommended that a physical or chemical treatment be employed to remove burnt residue in order to minimize channel wall roughness and enable precise channel dimension characterization. No specific treatment is recommended at this time.
- The experiment flow loop can be improved by replacing the accumulator, which has limited capacity, by a continuous flow micropump. This upgrade would allow testing for longer periods of time at elevated heat and flow rates.
- A system to control the inlet water temperature should be added to the flow loop. Pretreating the water by either cooling or heating would allow a consistent inlet temperature for the water delivered to the test section. In addition, the effect on inlet water temperature could be more readily ascertained.
- Flow measurements could potentially be upgraded by replacing the mass balance by a flow meter. The mass balance and stop watch method produces flow rate measurements with relatively low uncertainty. While more expensive, low mass flow rate meters may be able to produce the same level of uncertainty while streamlining the data acquisition process.

- Uncertainties in the reported data, such as *Re*, *Nu*, and *h*, could be reduced by using calibrated thermocouples.
- Decreasing the separation distance between adjacent sections of the spiral would increase overall channel length and heat transfer surface area at the expense of increasing required inlet pressures for an equivalent Reynolds number. Thus, it is suggested that tighter spiral patterns be investigated as a means to enhance the overall heat rate.
- Flow direction in this study was outward in the spiral. A reversed flow direction should be considered as secondary flow patterns would change, which may affect the overall heat rate.

To further advance the development of heat sinks fabricated by xurography, several recommendations are suggested:

- To enhance the microchannel heat sink thermal performance, a high thermal conductivity adhesive tape should be used.
- The channel hydraulic diameter and aspect ratio range could be extended by using different adhesive tape thicknesses (both thicker and thinner than that used in this study).
- Different substrate materials, such as aluminum and brass, could be used to fabricate the spiral microchannel heat sink. Machining these materials is easier than with copper. Thus, if one of the primary goals of creating a xurographic microchannel heat sink is quick turnaround time, it would be beneficial to use a material that is easier to machine. However, the thermal performance of a spiral heat sink fabricated from these materials would need to be determined.

- Working fluids other than distilled water could be used to extend the Reynolds number range, to study the effects of these fluids on the double-sided adhesive tape, and to study the fluid effect on leakage.
- Using lower inlet coolant temperatures would enhance thermal performance of the heat sink. It is suggested that thermal pretreatment of the coolant be studied as a means to enhance heat dissipation.
- Heat transfer rates can be improved at the expense of higher pressure drops if the flow rate is increased to the turbulent region. It is suggested that the Reynolds number range be extended to include the turbulent flow region.